

# Mixed-Valence Nickel–Iron Dithiolate Models of the [NiFe]-Hydrogenase Active Site

David Schilter,<sup>†</sup> Mark J. Nilges,<sup>†</sup> Mrinmoy Chakrabarti,<sup>‡</sup> Paul A. Lindahl,<sup>\*,‡</sup> Thomas B. Rauchfuss,<sup>\*,†</sup> and Matthias Stein<sup>\*,§</sup>

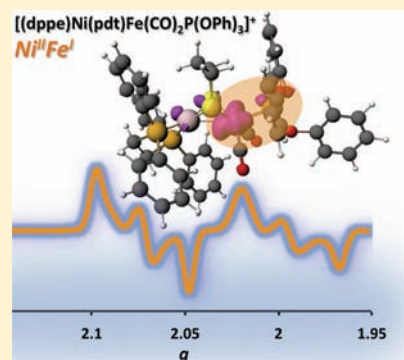
<sup>†</sup>Department of Chemistry, University of Illinois, 600 South Goodwin Avenue, Urbana, Illinois 61801, United States

<sup>‡</sup>Department of Chemistry, Texas A&M University, College Station, Texas 77842-3012, United States

<sup>§</sup>Max Planck Institute for Dynamics of Complex Technical Systems, Sandtorstrasse 1, 39106 Magdeburg, Germany

## Supporting Information

**ABSTRACT:** A series of mixed-valence nickel–iron dithiolates is described. Oxidation of (diphosphine)Ni(dithiolate)Fe(CO)<sub>3</sub> complexes **1**, **2**, and **3** with ferrocenium salts affords the corresponding tricarbonyl cations [(dppe)Ni(pdt)Fe(CO)<sub>3</sub>]<sup>+</sup> (**[1]<sup>+</sup>**), [(dppe)Ni(edt)Fe(CO)<sub>3</sub>]<sup>+</sup> (**[2]<sup>+</sup>**) and [(dcpe)Ni(pdt)Fe(CO)<sub>3</sub>]<sup>+</sup> (**[3]<sup>+</sup>**), respectively, where dppe = Ph<sub>2</sub>PCH<sub>2</sub>CH<sub>2</sub>PPh<sub>2</sub>, dcpe = Cy<sub>2</sub>PCH<sub>2</sub>CH<sub>2</sub>PCy<sub>2</sub>, (Cy = cyclohexyl), pdtH<sub>2</sub> = HSCH<sub>2</sub>CH<sub>2</sub>CH<sub>2</sub>SH, and edtH<sub>2</sub> = HSCH<sub>2</sub>CH<sub>2</sub>SH. The cation **[2]<sup>+</sup>** proved unstable, but the propanedithiolates are robust. IR and EPR spectroscopic measurements indicate that these species exist as C<sub>s</sub>-symmetric species. Crystallographic characterization of **[3]BF<sub>4</sub>** shows that Ni is square planar. Interaction of **[1]BF<sub>4</sub>** with P-donor ligands (L) afforded a series of substituted derivatives of type [(dppe)Ni(pdt)Fe(CO)<sub>2</sub>L]BF<sub>4</sub> for L = P(OPh)<sub>3</sub> (**[4a]BF<sub>4</sub>**), P(*p*-C<sub>6</sub>H<sub>4</sub>Cl)<sub>3</sub> (**[4b]BF<sub>4</sub>**), PPh<sub>2</sub>(2-py) (**[4c]BF<sub>4</sub>**), PPh<sub>2</sub>(OEt) (**[4d]BF<sub>4</sub>**), PPh<sub>3</sub> (**[4e]BF<sub>4</sub>**), PPh<sub>2</sub>(*o*-C<sub>6</sub>H<sub>4</sub>OMe) (**[4f]BF<sub>4</sub>**), PPh<sub>2</sub>(*o*-C<sub>6</sub>H<sub>4</sub>OCH<sub>2</sub>OMe) (**[4g]BF<sub>4</sub>**), P(*p*-tol)<sub>3</sub> (**[4h]BF<sub>4</sub>**), P(*p*-C<sub>6</sub>H<sub>4</sub>OMe)<sub>3</sub> (**[4i]BF<sub>4</sub>**), and PMePh<sub>2</sub> (**[4j]BF<sub>4</sub>**). EPR analysis indicates that ethanedithiolate **[2]<sup>+</sup>** exists as a single species at 110 K, whereas the propanedithiolate cations exist as a mixture of two conformers, which are proposed to be related through a flip of the chelate ring. Mössbauer spectra of **1** and oxidized S = 1/2 **[4e]BF<sub>4</sub>** are both consistent with a low-spin Fe(I) state. The hyperfine coupling tensor of **[4e]BF<sub>4</sub>** has a small isotropic component and significant anisotropy. DFT calculations using the BP86, B3LYP, and PBE0 exchange–correlation functionals agree with the structural and spectroscopic data, suggesting that the SOMOs in complexes of the present type are localized in an Fe(I)-centered d(z<sup>2</sup>) orbital. The DFT calculations allow an assignment of oxidation states of the metals and rationalization of the conformers detected by EPR spectroscopy. Treatment of **[1]<sup>+</sup>** with CN<sup>−</sup> and compact basic phosphines results in complex reactions. With dppe, **[1]<sup>+</sup>** undergoes quasi-disproportionation to give **1** and the diamagnetic complex [(dppe)Ni(pdt)Fe(CO)<sub>2</sub>(dppe)]<sup>2+</sup> (**[5]<sup>2+</sup>**), which features square-planar Ni linked to an octahedral Fe center.

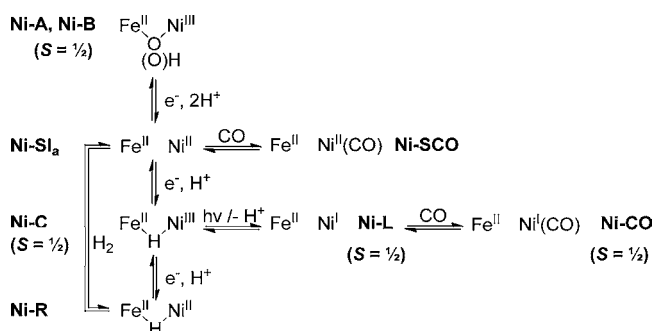


## INTRODUCTION

The modeling of the active sites of the hydrogenases (H<sub>2</sub>ases) is a fertile area for research because the inorganic chemistry at play is unusual. Most distinctive is the prevalence of paramagnetic states; this contrasts the chemistry of metal carbonyls in which open shell species are uncommon. Why have H<sub>2</sub>ases adopted S = 1/2 states, especially given that the H<sub>2</sub>/H<sup>+</sup> redox process involves 2e<sup>−</sup>? While good progress has been made on modeling the paramagnetic states of the [FeFe]-H<sub>2</sub>ases,<sup>1–3</sup> synthetic analogs for the corresponding odd-electron states of the [NiFe]-H<sub>2</sub>ases have not been characterized as well.

The active sites of [NiFe]-H<sub>2</sub>ases exist in several S = 1/2 states, but only the Ni-C state (Scheme 1)<sup>4</sup> is implicated in the catalytic mechanism.<sup>5</sup> Spectroscopic analysis of the Ni-C state indicates a Ni(III)Fe(II) center bridged by a hydrido ligand.<sup>6,7</sup> Upon irradiation at low-temperatures, Ni-C converts to Ni-L (Scheme 2), another S = 1/2 state first observed in enzymes from *Allochrochromatium vinosum*.<sup>8</sup> Spectroscopic analysis and DFT

## Scheme 1

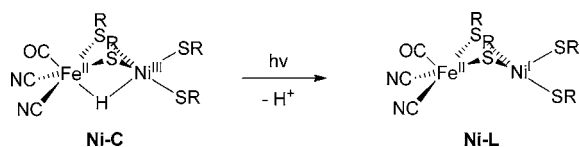


calculations indicate a Ni(I)Fe(II) core in which the hydrido bridge is absent. Thus, Ni-C undergoes a photoreduction in

Received: October 27, 2011

Published: February 3, 2012

Scheme 2



which the two-electron more reduced Ni-L is reached. Photoconversion appears to involve the deprotonation of Ni-C by a proximal base that has not been identified.<sup>9</sup> EPR and ENDOR experiments and DFT calculations on the Ni-L state have shown that the majority of the unpaired spin density is localized at the Ni center, consistent with a Ni(I)Fe(II) oxidation state assignment.

Ni-A (unready) and Ni-B (ready) are more oxidized  $S = 1/2$  states of  $H_2$ ases, both with Ni(III)Fe(II) cores. High-resolution crystallographic studies have been reported for the enzymes from *Desulfovibrio gigas* (85% Ni-A/15% Ni-B),<sup>10</sup> *Desulfovibrio fructosovorans* (Ni-B),<sup>11</sup> *Desulfovibrio vulgaris* Miyazaki F (Ni-B,<sup>12</sup> Ni-SI/Ni-R),<sup>13</sup> and *Desulfovibrio desulfuricans* (Ni-B).<sup>14</sup> Regardless of the state of the enzyme, the active site consists of Ni coordinated to four thiolato (or thiol) ligands, two of which bridge to an “organometallic”  $Fe(CN)_2(CO)$  fragment.<sup>15</sup> Although the first crystal structure of [NiFe]- $H_2$ ase appeared in 1995, synthetic modeling of this family of hydrogenases has only recently afforded complexes with structures approaching this active site.

Synthetic models featuring a NiFe core in which Ni(II) is bound by four sulfur ligands have been reported by the Tatsumi group (Figure 1, left).<sup>16</sup> This dithiocarbamate complex, in

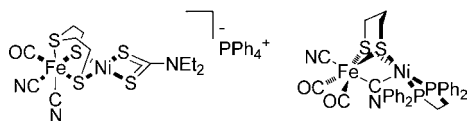
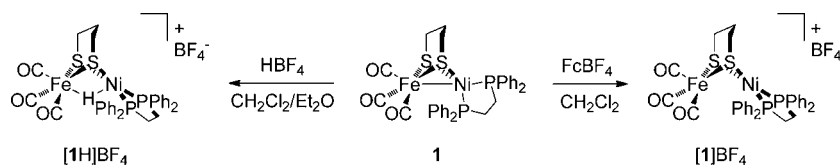


Figure 1. Structural mimics of the active site of the [NiFe]- $H_2$ ases.

addition to reproducing the Ni coordination environment, also features the  $Fe(CN)_2(CO)$  fragment, albeit bound to a thioether. The CN and CO bands in the IR spectrum match those of the enzyme in the unready Ni-A state, suggesting that the Fe(II) centers in the model complex and [NiFe]- $H_2$ ase have similar electron densities. Such  $34e^-$  complexes may be considered models for Ni-SCO, an EPR-silent, CO-bound,  $H^-$ -free state of [NiFe]- $H_2$ ase in which the Ni and Fe centers are in the +2 oxidation state.<sup>17</sup> A key difference, however, can be found in the Ni and Fe coordination numbers: in such models these are 4 and 6, respectively, whereas in Ni-SCO the extrinsic CO binds Ni, causing both centers to be 5-coordinate.

Jiang and co-workers have prepared a related Ni(II)Fe(II) structural model (Figure 1, right) that incorporates a  $Fe(CN)_2(CO)_2$  fragment bridged to Ni by a pair of thiolate ligands.<sup>18</sup> This complex is closely related to the dithiocarbamate example,

Scheme 3



although an additional CO replaces the thioether at the Fe(II) center and the chelating diphosphine dppe is used in place of the dithiocarbamate. Dppe has also been employed as a surrogate for terminal thiolates in  $[(dppe)Ni(pdt)Fe(CO)_3]$  (**1**), a model described by Schröder and co-workers.<sup>19</sup> In contrast to the models discussed above, the Fe center is bound to only three ligands besides the bridging thiolates. This derivative features metal–metal bonding absent in more oxidized NiFe complexes such as those described by Tatsumi, Jiang, and their co-workers.

The formally Ni(I)Fe(I) species **1** readily protonates to furnish the conjugate acid  $[(dppe)Ni(pdt)(\mu-H)Fe(CO)_3]BF_4$  ( $[1H]BF_4$ ), which features a hydrido ligand bridging the Ni(II) and Fe(II) centers (Scheme 3).<sup>20</sup> This complex was the first hydride of a NiFe thiolate, and the significance of this stoichiometric resemblance is enhanced by this complex's ability to catalyze the reduction of protons to  $H_2$ . More recently, the Fe coordination sphere has been varied to afford more electron-rich derivatives of type  $[(dppe)Ni(pdt)(\mu-H)Fe(CO)_2(PR_3)]^+$ .<sup>21</sup> This family of hydrido complexes represent promising models for the Ni–R state of [NiFe]- $H_2$ ase, which is characterized by an  $S = 0$  Ni(II)Fe(II) core with a proposed bridging hydrido ligand.<sup>13</sup>

In a preliminary communication, we reported that oxidation of the neutral complex **1** using a ferrocenium salt ( $FcBF_4$ ) allowed for the *in situ* preparation of  $[(dppe)Ni(pdt)Fe(CO)_3]BF_4$  ( $[1]BF_4$ ), which was characterized by IR and EPR spectroscopy.<sup>20</sup> This salt remains the only potential mimic of a paramagnetic state of the enzyme. In this paper, we describe the synthesis of a series of  $S = 1/2$  NiFe carbonyls, the first models for Ni-L. Such compounds have spin distributions inverse to that of Ni-L, and their characterization sheds new light on the role of the ligands in fine-tuning electronic structure of bimetallic species. Additionally, our studies revealed the tendency of some members of this series to undergo disproportionation, thereby affording potential models for Ni-SCO state.

## RESULTS

$[(Diphosphine)Ni(pdt)Fe(CO)_3]^+$ . Preliminary studies revealed that  $(dppe)Ni(pdt)Fe(CO)_3$  (**1**) and related complexes undergo oxidation at approximately  $-0.5$  V vs  $Fc^{+/0}$ . For this reason, the new cations were prepared from the neutral Ni(I)-Fe(I) complexes and  $FcBF_4$ . The first example of the series is  $[1]BF_4$ , which could be isolated as a brown powder. This salt dissolves in  $CH_2Cl_2$  to give moderately stable solutions, which are unaffected by ambient light but are sensitive to  $O_2$  and  $H_2O$ . Solutions in THF and MeCN decompose to unidentified products. Using the appropriate ferrocenium salts, we also prepared solutions of  $[1]BAR_4^+$  ( $BAR_4^- =$  tetrakis(3,5-bis(trifluoromethyl)phenyl)borate) and  $[1]PF_6$ . The latter could be isolated as a brown powder. Although the solubility properties of these salts varied, their IR and EPR spectra (see below) were very similar.

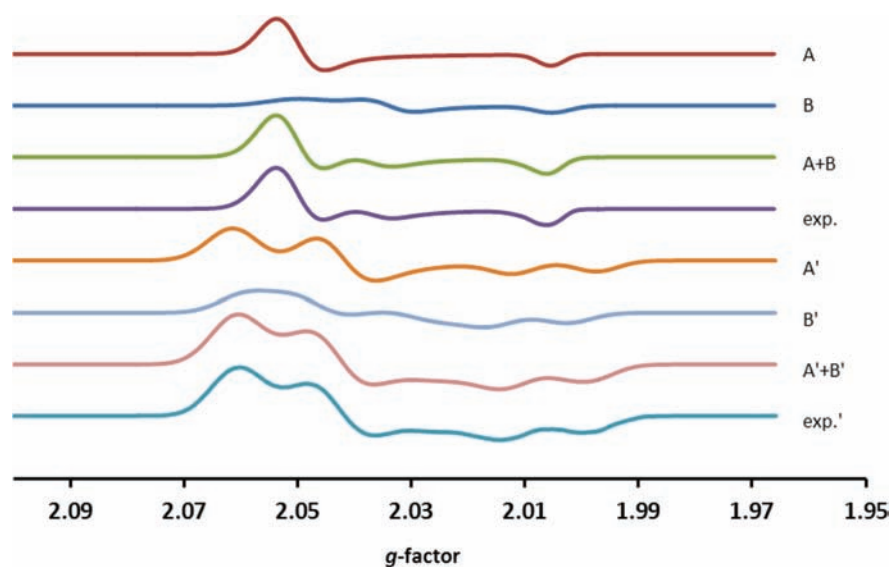


**Figure 2.** X-band EPR spectra ( $\text{CH}_2\text{Cl}_2/\text{PhMe}$ , 110 K) of  $[\mathbf{1}]\text{BF}_4$  (exp.) and  $[\mathbf{1}']\text{BF}_4$  (exp.'). In each case the experimental spectrum could be simulated as sum of two components, denoted A+B (for  $[\mathbf{1}]\text{BF}_4$ ), and A'+B' (for  $[\mathbf{1}']\text{BF}_4$ ).

Under  $^{13}\text{CO}$  (1 atm), **1** in  $\text{CH}_2\text{Cl}_2$  solution converted to  $[(\text{dppe})\text{Ni}(\text{pdt})\text{Fe}(^{13}\text{CO})_3]$  (**1'**), for which the  $\nu_{\text{CO}}$  bands are shifted to lower energies (1982 (m), 1913 (s)  $\text{cm}^{-1}$  vs 2028 (m), 1932 (s)  $\text{cm}^{-1}$ ). Similarly,  $[\mathbf{1}]\text{BF}_4$  also exchanges with  $^{13}\text{CO}$ , allowing for the generation of  $[(\text{dppe})\text{Ni}(\text{pdt})\text{Fe}(^{13}\text{CO})_3]\text{BF}_4$  ( $[\mathbf{1}']\text{BF}_4$ ), which has  $\nu_{\text{CO}}$  bands consistent with complete labeling (2009 (m), 1941 (s)  $\text{cm}^{-1}$  vs 2057 (m), 1986 (s)  $\text{cm}^{-1}$ ). Analogously to the parent complex, the labeled salt can also be prepared by the oxidation of  $[(\text{dppe})\text{Ni}(\text{pdt})\text{Fe}(^{13}\text{CO})_3]$  (**1'**) with  $\text{FcBF}_4$ .

The X-band EPR spectrum of a frozen  $\text{CH}_2\text{Cl}_2/\text{PhMe}$  solution of  $[\mathbf{1}]\text{BF}_4$  (Figure 2, exp.) exhibits two comparably intense signals, including an axial signal (A) and rhombic signal (B). These signals are consistent with the presence of two isomers. The absence of any resolved  $^{31}\text{P}$  hyperfine coupling indicates that negligible spin density resides on the Ni center, suggesting a Fe(I)Ni(II) oxidation state. This assignment was further confirmed by comparing this spectrum to that of the  $^{13}\text{C}$ -labeled compound  $[\mathbf{1}']\text{BF}_4$  (exp.'). The EPR spectrum of the latter again suggests the presence of two closely related isomers with signals split by a single  $I = 1/2$  nucleus ( $A = 62, 53, 72$  MHz), proposed to be the apical  $^{13}\text{C}$  atom. One signal was further split/broadened ( $A = 13, 30, 17$  MHz) owing to weak interactions with the two equivalent basal  $^{13}\text{CO}$  ligands. For comparison, the coupling observed for the Fe(I)- $^{13}\text{CO}$  spin system in the  $\text{H}_{\text{ox}}$  state of  $[\text{FeFe}]\text{-H}_2\text{ase}$  is 21 MHz.<sup>22</sup> EPR spectra for  $[\mathbf{1}]\text{BF}_4$ ,  $[\mathbf{1}]\text{PF}_6$ , and  $[\mathbf{1}]\text{BARF}_4$  were similar.

Two analogs of  $[\mathbf{1}]^+$  were examined involving replacement of the dithiolate and the diphosphine. Oxidation of ethanedithiolate  $[(\text{dppe})\text{Ni}(\text{edt})\text{Fe}(\text{CO})_3]$  (**2**)<sup>23</sup> with ferrocenium salts gave unstable products regardless of the counteranion. *In situ* IR analysis of these solutions confirmed that the cation  $[\mathbf{2}]^+$  ( $\nu_{\text{CO}} = 2059$  (m), 1988 (s)  $\text{cm}^{-1}$ ) closely resembles  $[\mathbf{1}]^+$ , although these solutions also contained significant amounts of **2** and  $[\mathbf{2H}]^+$ . The instability of  $[\mathbf{2}]^+$  contrasts with the good stability of the corresponding hydrido complex  $[\mathbf{2H}]^+$ , whose structure is expected to closely resemble that of the mixed-valence derivative. The EPR analyses of  $[\mathbf{2}]^+$  are discussed later. Lastly, oxidation of the more electron-rich complex  $[(\text{dcpe})\text{Ni}(\text{pdt})\text{Fe}(\text{CO})_3]$  (**3**) with  $\text{FcBF}_4$  in  $\text{CH}_2\text{Cl}_2$  solution afforded

$[\mathbf{3}]\text{BF}_4$ , which is similar to  $[\mathbf{1}]\text{BF}_4$  in terms of its spectroscopy (Figures S14, S15, Supporting Information) and stability.

**Structure of  $[(\text{dcpe})\text{Ni}(\text{pdt})\text{Fe}(\text{CO})_3]\text{BF}_4$ .** X-ray crystallography allowed for structural confirmation of  $[\mathbf{3}]\text{BF}_4$ , the results of which are presented in Figure 3.

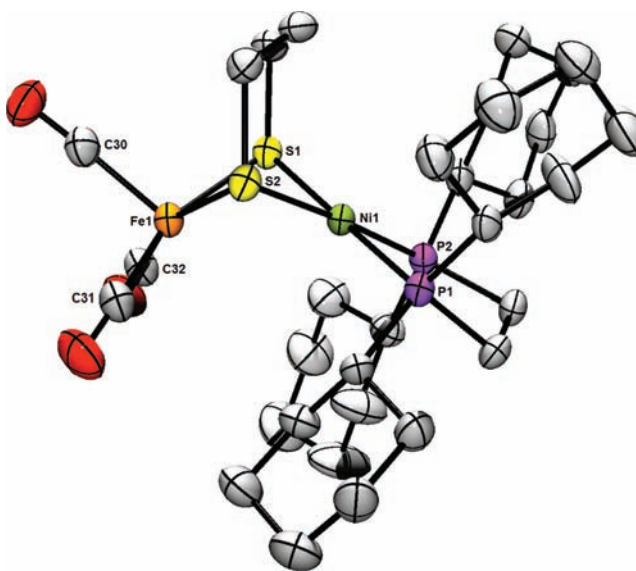


**Figure 3.** ORTEP of  $[\mathbf{3}]\text{BF}_4$  with ellipsoids drawn at the 50% probability level. The H atoms,  $\text{BF}_4^-$  anion, and two  $\text{CH}_2\text{Cl}_2$  solvate molecules are omitted for clarity. Selected distances ( $\text{\AA}$ , distances calculated using BP/TZVP are given in parentheses): Ni1–Fe1, 2.818 (2.76); Ni1–P1, 2.191 (2.23); Ni1–P2, 2.188 (2.22); Ni1–S1, 2.235 (2.25); Ni1–S2, 2.227 (2.24); Fe1–S1, 2.296 (2.31); Fe1–S2, 2.288 (2.34); Fe1–C30, 1.833 (1.80); Fe1–C31, 1.799 (1.79); Fe1–C32, 1.790 (1.79).

The Ni–Fe distance in  $[\mathbf{3}]\text{BF}_4$  (2.818  $\text{\AA}$ ) is longer than that in **1** (2.467  $\text{\AA}$ ), as well as the Ni(II)( $\mu\text{-H}$ )Fe(II) complex  $[\mathbf{3H}]\text{BF}_4$  (2.684  $\text{\AA}$ ), in which a hydrido ligand is present. Whereas the atom connectivity in **3** and  $[\mathbf{3}]^+$  is identical, a dramatic conformational change occurs upon oxidation. The Ni center in  $[\mathbf{3}]\text{BF}_4$  exists in an almost square planar coordination environment, as indicated by the twist angle of 3.55° between

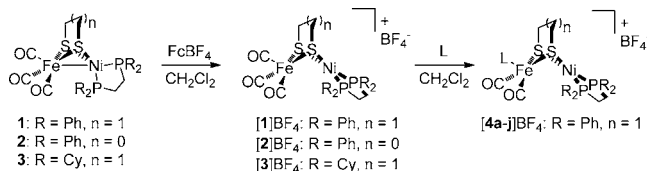


the NiP<sub>2</sub> and NiS<sub>2</sub> planes. In contrast, the Ni center in **3** is thought to be tetrahedral, the relevant twist angle in the closely related dppe analog **1** being 84.91°. By comparison, the (dcpe)Ni(pdt) fragment in [3H]BF<sub>4</sub> is also almost square planar, and the average Ni–P distance for this complex (2.189 Å)<sup>20</sup> is identical to that in [3]BF<sub>4</sub>.<sup>21</sup> The solid-state data are consistent with [3]BF<sub>4</sub> featuring a Ni(II) center. The Fe center is situated in an approximately square-pyramidal environment, with C30 occupying the apical position. Such a geometry is often adopted by mononuclear Fe(I)<sup>24</sup> and dinuclear Fe(I)Fe(II) compounds.<sup>25,26</sup> The Fe–C<sub>basal</sub> distances (1.799, 1.790 Å) are somewhat shorter than the Fe–C<sub>apical</sub> distance (1.833 Å), as might be expected for a complex with CO ligands *trans* to strong  $\sigma$ -donors. Furthermore, the average Fe–C distance in [3]BF<sub>4</sub> (1.807 Å) is similar to that for **1** (1.798 Å), consistent with the Fe centers in both complexes being in the same +1 oxidation state.

**Substituted Derivatives of [1]<sup>+</sup>**. In an attempt to introduce CN<sup>−</sup> ligands, a solution of [1]BAR<sup>F</sup> was treated with NBu<sub>4</sub>CN. However, this reaction afforded **1** as the predominant species according to IR analysis. The redox process was rapid and accompanied by effervescence, believed to result from evolution of NCCN. The formation of **1** was also observed when [1]BF<sub>4</sub> was treated with either the *N*-heterocyclic carbene bis(2,6-diisopropylphenyl)imidazolin-2-ylidene or the isocyanide MeNC.

Given the propensity of C-donors to reduce [1]<sup>+</sup>, less basic ligands were investigated. Addition of [1]BF<sub>4</sub> to an excess of PPh<sub>3</sub> in CH<sub>2</sub>Cl<sub>2</sub> solution resulted in evolution of CO and formation of a dark red-brown solution. The reaction was instantaneous, and a red-brown powder could be precipitated with pentane. The IR spectrum of this product features a pair of comparably intense  $\nu_{\text{CO}}$  bands at 1988 and 1929 cm<sup>−1</sup>, consistent with the formation of the monosubstituted *cis*-dicarbonyl species [(dppe)Ni(pdt)Fe(CO)<sub>2</sub>PPh<sub>3</sub>]BF<sub>4</sub> ([4e]BF<sub>4</sub>) according to Scheme 4. The mean shift in  $\nu_{\text{CO}}$  upon

#### Scheme 4



substitution is  $-63$  cm<sup>−1</sup> relative to the tricarbonyl parent compound [1]BF<sub>4</sub> ( $\nu_{\text{CO}}$  = 2057, 1986 cm<sup>−1</sup>). An identical shift in  $\nu_{\text{CO}}$  was observed upon replacement of one CO for PPh<sub>3</sub> in [1H]BF<sub>4</sub> to give [(dppe)Ni(pdt)( $\mu$ -H)Fe(CO)<sub>2</sub>PPh<sub>3</sub>]BF<sub>4</sub>.<sup>21</sup> Further information regarding the identity of [4e]BF<sub>4</sub> was gleaned from its positive-ion ESI mass spectrum, which featured a base peak at *m/z* 936.3 for the parent ion [4e]<sup>+</sup>.

Analogous to the preparation of [4e]BF<sub>4</sub>, a range of other monosubstituted derivatives were prepared ([4a–j]BF<sub>4</sub>), each of which was characterized according to analytical and ESI-MS data, as well as by IR and EPR spectroscopy. ESI-MS analyses supported the formulation of the new complexes as [(dppe)Ni(pdt)Fe(CO)<sub>2</sub>L]<sup>+</sup>. Ionization by loss of BF<sub>4</sub><sup>−</sup> from the salts allowed for the detection of the parent ions, with the isotopic distributions being consistent with their structures. In some cases significant fragmentation was also observed, in which the cations lose a terminal ligand to afford species of the type [(diphosphine)Ni(dithiolate)Fe(CO)<sub>2</sub>]<sup>+</sup> and [(dppe)Ni(pdt)Fe(CO)L]<sup>+</sup>.

The  $\nu_{\text{CO}}$  values for the compounds prepared are given in Table 1. These data correlate inversely with the basicity of the

**Table 1.** IR Data for Compounds of Type [(dppe)Ni(pdt)Fe(CO)<sub>2</sub>L]BF<sub>4</sub> in CH<sub>2</sub>Cl<sub>2</sub> Solution, Ordered in Decreasing  $\nu_{\text{CO}}$ <sup>a</sup>

L	compound	$\nu_{\text{CO}}$ , cm <sup>−1</sup>	TEP, cm <sup>−1</sup>
P(OPh) <sub>3</sub>	[4a]BF <sub>4</sub>	2007, 1952	2085.3
	[4a']BF <sub>4</sub>	1961, 1907	
P( <i>p</i> -C <sub>6</sub> H <sub>4</sub> Cl) <sub>3</sub>	[4b]BF <sub>4</sub>	1991, 1933	2072.8
	[4c]BF <sub>4</sub>	1990, 1932	
PPh <sub>2</sub> (2-py)	[4d]BF <sub>4</sub>	1989, 1929	2068.9
	[4e]BF <sub>4</sub>	1988, 1929	
PPh <sub>2</sub> (OEt)	[4f]BF <sub>4</sub>	1941, 1885	2066.1
	[4g]BF <sub>4</sub>	1987, 1928	
PPh <sub>2</sub> ( <i>o</i> -C <sub>6</sub> H <sub>4</sub> OMe)	[4f]BF <sub>4</sub>	1987, 1929	2066.1
	[4g]BF <sub>4</sub>	1987, 1928	
PPh <sub>2</sub> ( <i>o</i> -C <sub>6</sub> H <sub>4</sub> OCH <sub>2</sub> OMe)	[4f]BF <sub>4</sub>	1985, 1927	2066.7
	[4i]BF <sub>4</sub>	1985, 1926	
P( <i>p</i> -tol) <sub>3</sub>	[4h]BF <sub>4</sub>	1985, 1926	2066.1
	[4j]BF <sub>4</sub>	1985, 1977, 1928, 1907	
P( <i>p</i> -C <sub>6</sub> H <sub>4</sub> OMe) <sub>3</sub>	[4i]BF <sub>4</sub>	1985, 1926	2066.1
	[4j]BF <sub>4</sub>	1985, 1977, 1928, 1907	
PMePh <sub>2</sub>	[4j]BF <sub>4</sub>	1985, 1977, 1928, 1907	2067.1
	[4j]BF <sub>4</sub>	1985, 1977, 1928, 1907	

<sup>a</sup>Data for the <sup>13</sup>CO-labeled analogs, [(dppe)Ni(pdt)Fe(<sup>13</sup>CO)<sub>2</sub>L]BF<sub>4</sub>, are included, these compounds being denoted with prime symbols.

monodentate *P*-donor ligands employed. As expected, the trend in  $\nu_{\text{CO}}$  values roughly mirrors the trend in the Tolman Electronic Parameter<sup>27</sup> (TEP) for each *P*-donor ligand. The similarity of the IR data for complexes of PPh<sub>3</sub>, PPh<sub>2</sub>(2-py) ([4c]BF<sub>4</sub>), PPh<sub>2</sub>(*o*-C<sub>6</sub>H<sub>4</sub>OMe) ([4f]BF<sub>4</sub>), and PPh<sub>2</sub>(*o*-C<sub>6</sub>H<sub>4</sub>OCH<sub>2</sub>OMe) ([4g]BF<sub>4</sub>) indicates that ether and pyridyl substituents do not interact significantly with the metal centers in the monocations.

In many cases, the two  $\nu_{\text{CO}}$  bands have discernible shoulders at lower energy, suggesting that the complexes are present as two species in solution. This effect is most pronounced in the case of the PMePh<sub>2</sub> complex ([4j]BF<sub>4</sub>), where the absorptions can be somewhat resolved (Figure S48, Supporting Information). The isomerism involved is addressed in the following section.

**EPR Spectroscopy of [(dppe)Ni(pdt)Fe(CO)<sub>2</sub>L]<sup>+</sup>**. All substituted mixed-valence derivatives were characterized by X-band EPR spectroscopy; selected spectra were simulated in order to extract *g* and *A*(<sup>31</sup>P) values, which are presented in Table 2. Spectra not presented here can be found in the Supporting Information.

The EPR spectrum of the PPh<sub>3</sub>-containing compound [4e]BF<sub>4</sub> (Figure 4) features a pattern of two overlapping rhombic signals, consistent with the lower symmetry of [4e]<sup>+</sup> relative to [1]<sup>+</sup>. The hyperfine splitting of the signals is attributed to the coupling to the PPh<sub>3</sub> ligand, the associated *A* values being in the range 117–217 MHz. Spectra for [4a–j]BF<sub>4</sub> are similar. BP/TZP calculations predict a large isotropic hyperfine coupling of +202 MHz for <sup>31</sup>PPh<sub>3</sub> in [4e]<sup>+</sup> and a dipolar contribution of (−17, −16, +33) MHz. The hyperfine coupling to the dppe *P* nuclei is significantly weaker (*A*<sub>iso</sub> = 4 MHz).

The <sup>13</sup>CO-labeled derivative [(dppe)Ni(pdt)Fe(<sup>13</sup>CO)<sub>2</sub>PPh<sub>3</sub>]BF<sub>4</sub> ([4e']BF<sub>4</sub>, prepared from [1']), was studied in order to derive further structural information about complexes of the present type. In their EPR spectra, the *g*-values for [4e]BF<sub>4</sub> and [4e']BF<sub>4</sub> are almost identical (Table 2). In addition to the <sup>31</sup>P coupling arising from Fe-bound PPh<sub>3</sub>, further signal broadening is observed in the case of [4e']BF<sub>4</sub>, a result of weak interactions with the two <sup>13</sup>CO ligands (Figure S35, Supporting Information). The data suggest that in such arrangements a

Table 2. EPR Simulation Parameters for Salts of Mixed-Valence Complexes<sup>a</sup>

compound	g-factor	A( <sup>31</sup> P) (MHz)	line width (G)	relative abundance
[1]BF <sub>4</sub>	2.052, 2.050, 2.005		13, 18, 12	0.57
	2.055, 2.038, 2.009		14, 17, 13	0.43
[1']BF <sub>4</sub>	2.053, 2.051, 2.005 <sup>b</sup>		11, 11, 7	0.62
	2.054, 2.037, 2.008 <sup>c</sup>		16, 11, 10	0.38
[2]BF <sub>4</sub>	2.054, 2.053, 2.010	18, 15, 16	5, 11, 4	
[4a]BF <sub>4</sub>	2.058, 2.031, 2.007	345, 345, 364	8, 10, 6	0.68
	2.053, 2.051, 2.004	351, 311, 372	14, 20, 6	0.32
[4a']BF <sub>4</sub>	2.058, 2.032, 2.007 <sup>d</sup>	345, 345, 364	8, 10, 6	0.68
	2.053, 2.051, 2.004 <sup>e</sup>	351, 311, 372	14, 20, 6	0.32
[4e]BF <sub>4</sub>	2.066, 2.036, 2.006	167, 165, 211	6, 13, 10	0.77
	2.066, 2.045, 2.004	177, 147, 211	22, 5, 11	0.23
[4e']BF <sub>4</sub>	2.066, 2.038, 2.006 <sup>f</sup>	168, 183, 195	10, 13, 8	0.66
	2.070, 2.042, 2.007 <sup>g</sup>	152, 117, 227	12, 20, 6	0.34
[4h]BF <sub>4</sub>	2.064, 2.036, 2.004	170, 182, 197	11, 13, 8	0.66
	2.069, 2.037, 2.004	147, 122, 228	13, 20, 6	0.34

<sup>a</sup>Where two entries exist for a given compound, two isomers are represented, the relative abundances of which are given in the last column. Parameters for [4a]BF<sub>4</sub> were derived from both X- and Q-band data. <sup>b</sup>A(<sup>13</sup>C) = 62, 53, 72 and 13, 30, 17. <sup>c</sup>A(<sup>13</sup>C) = 57, 80, 50 (coupling for basal <sup>13</sup>C unresolved). <sup>d</sup>A(<sup>13</sup>C) = 16, 19, 20. <sup>e</sup>A(<sup>13</sup>C) = 12, 12, 20. <sup>f</sup>A(<sup>13</sup>C) = 18, 17, 23. <sup>g</sup>A(<sup>13</sup>C) = 20, 14, 22.

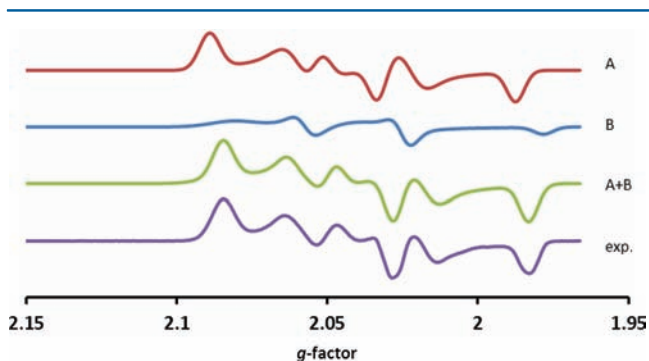


Figure 4. X-band EPR spectra (CH<sub>2</sub>Cl<sub>2</sub>/PhMe, 110 K) of [4e]BF<sub>4</sub>. The experimental spectrum (exp.) could be simulated as the sum of two components, denoted A+B.

ligand must be in the apical position to interact strongly with the Fe-centered SOMO.

The compound [4a]BF<sub>4</sub> is noteworthy owing to its high A<sub>p</sub> values, which average 354 and 345 MHz for the axial and rhombic components (2:1), respectively (Figure 5). These values

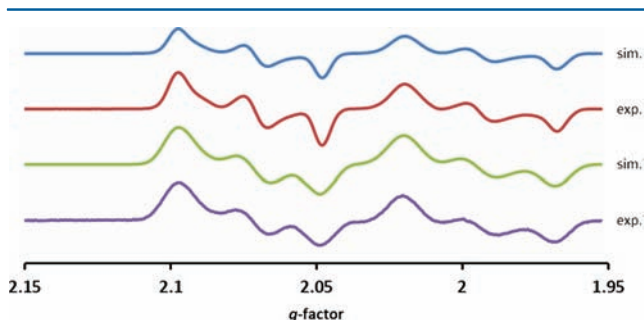


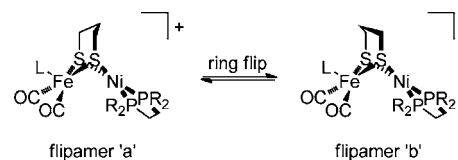
Figure 5. X-band EPR spectra (CH<sub>2</sub>Cl<sub>2</sub>/PhMe, 110 K) of [4a]BF<sub>4</sub> (exp.) and [4a']BF<sub>4</sub> (exp.). Simulated spectra (sim. and sim.', respectively) are also presented.

suggest significant spin delocalization onto the P(OPh)<sub>3</sub> ligand, which is the best π-acceptor of the P-donor ligands employed. The <sup>13</sup>CO-labeled compound [4a']BF<sub>4</sub> was prepared to clarify the assignment. As with the PPh<sub>3</sub> congener [4e']BF<sub>4</sub>, the presence

of <sup>13</sup>CO ligands results in only slight signal broadening, suggesting that the P(OPh)<sub>3</sub> ligand is apically bound to Fe(I), with the basal <sup>13</sup>CO ligands interacting only weakly with the SOMO.

EPR spectra of the Ni(II)Fe(I) compounds [1]BF<sub>4</sub>, [3]BF<sub>4</sub>, and [4a–j]BF<sub>4</sub> (and the <sup>13</sup>CO-labeled analogs prepared) indicate, in each case, the presence of two species. For [4a–j]BF<sub>4</sub>, these isomers have almost identical EPR parameters. Indeed, satisfactory simulations could only be obtained when two species were considered. It is suggested that these species are very similar, and the data are consistent with the isomers being related by a ring flip of the bridging pdt<sup>2-</sup> ligand (Scheme 5).

#### Scheme 5



The presence of two isomers is more pronounced when the room temperature spectra are considered (selected spectra presented in Supporting Information), suggesting a slow interconversion between conformers (“flipamers”). Additionally, the dispersion afforded by Q-band EPR was exploited in the analysis of one example, [4e]BF<sub>4</sub>. In this case, the high-field (*g<sub>z</sub>*) resonance has obvious shoulders, which are evident in one of the two modeled signals (Figure S32, Supporting Information).

The existence of flipamers is found in pdt-bridged dinuclear species, the ring inversion/flipping barriers typically being 8–11 kcal/mol.<sup>28,29</sup> For example, EPR spectroscopy was used to detect the two flipamers of the [FeFe]-H<sub>2</sub>ase model complex [(dppv)(CO)Fe(pdt)Fe(CO)<sub>2</sub>(PMe<sub>3</sub>)]<sup>+</sup> (dppv = *cis*-1,2-bis(diphenylphosphino)ethene).<sup>25</sup>

This isomerism is not possible for the ethanedithiolate cation [2]<sup>+</sup>, and although it was too unstable to be isolated as a salt, EPR analysis was conducted on a sample prepared *in situ*. The spectrum recorded at 110 K (Figure 6) revealed an almost purely axial signal, corresponding to a single spin system. The signal at higher field is split into a triplet, whereas the hyperfine splitting of the low-field resonance is unresolved.

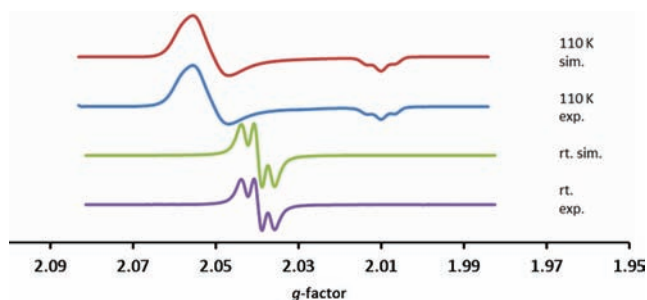


**Figure 6.** X-band EPR spectra ( $\text{CH}_2\text{Cl}_2/\text{PhMe}$ ) of  $[\mathbf{2}]\text{BF}_4$  collected at 110 K (110 K exp.) and room temperature (rt exp.). Simulated spectra are also presented.

Coupling ( $A = 14$  MHz) was also observed in the room temperature isotropic spectrum, again implying the presence of a single species in which an unpaired electron is coupled to two equivalent  $I = 1/2$  nuclei. Such a signal arises either from the coupling of an Fe(I) center with two protons on the  $\text{edt}^{2-}$  ligand or a Ni(I)– $^{31}\text{P}$  interaction; this question is addressed in the following section. The fact that this complex is present as a single species in solution is consistent with the two EPR signals from  $[\mathbf{1}]\text{BF}_4$  arising from the presence of flipamers.

**DFT Calculations.** Density functional theoretical calculations were performed in an effort to rationalize EPR data and assign the oxidation states. The calculations support the assignments of Ni(I)Fe(I) for the neutral complexes and Ni(II)Fe(I) for the singly oxidized derivatives. The calculated structural parameters agree with those determined experimentally to within 0.01 Å for bond lengths and  $1\text{--}2^\circ$  for bond angles. The structure calculated for  $[\mathbf{1}]^+$  (Figure 7) is very similar to that observed crystallographically for  $[\mathbf{3}]^+$ , with the Ni–Fe distances being 2.818 and 2.80 Å, respectively.

With the observed structure, the Mulliken population of the unpaired spin on Fe is 0.72 and on Ni is 0.12 (see Figure 7). Upon ring inversion of  $\text{pdt}^{2-}$  chelate ring, the distribution of the unpaired spin density remains nearly unchanged, but small differences in  $g$ -values are detectable (*vide infra*).

The calculated  $g$ -tensor principal values from the spin-unrestricted CP-SCF calculations and spin-restricted ZORA calculations give a consistent picture of the electronic structure of the mixed-valence NiFe dithiolates. The  $g$ -values reported for Ni–L (2.30, 2.12, 2.05), in particular the deviation of the  $g_z$

component from  $g_e$  (2.0023), are indicative of the presence of Ni(I) in this state of the enzyme. Calculations using the BP86 (Becke exchange, Perdew correlation),<sup>30,31</sup> B3LYP (Becke exchange, Lee–Yang–Parr correlation),<sup>32</sup> and PBE0 (Perdew, Burke and Ernzerhof)<sup>33,34</sup> hybrid functionals give  $g$ -tensors for the compounds  $[\mathbf{1}]^+$ ,  $[\mathbf{2}]^+$ ,  $[\mathbf{3}]^+$ ,  $[\mathbf{4a}]^+$ , and  $[\mathbf{4e}]^+$  (Table 1 of the Supporting Information) in which the smallest  $g$ -component,  $g_3$ , is close to  $g_e$ , effectively ruling out Ni(I) species.

In general BP86 tends to underestimate  $g$ -shifts by about 19 ppt for  $g_1$ , whereas PBE0 tends to slightly overestimate  $g$ -shifts. Best agreement with experiment is obtained with the B3LYP hybrid functional. The self-consistent consideration of spin–orbit coupling in spin-restricted calculations with Slater basis functions gives larger  $g$ -shifts compared with the effective potential approach through the coupled-perturbed SCF equation. The calculations are accurate enough to assign the two conformers (see Scheme 5). For example, the experimental  $g$ -tensors for  $[\mathbf{1}]^+$  (2.052, 2.050, 2.005 and 2.055, 2.038, 2.009) can be compared with those derived computationally (ZORA, B3LYP). Calculations suggest that axial  $g$ -values (2.052, 2.051, 2.006) can be expected when the central  $\text{CH}_2$  is oriented toward Ni (flipamer a). Slightly lower  $g$ -values can be observed (2.051, 2.047, 2.005) when this group is instead closer to Fe (as it is in flipamer b). Whereas  $g_1$  remains almost unchanged, the largest decrease occurs for  $g_2$ . This effect can be rationalized by the  $g_2$ -axis pointing toward the thiolate bridging ligand and being thus sensitive to the orientation of the  $\text{pdt}^{2-}$  ligand. In two cases, the relative energies between flipamers and their barrier to interconversion were computed. For the tricarbonyl complex  $[\mathbf{1}]^+$ , the Gibbs free energy of flipamer ‘a’ is lower by 1 kcal/mol, the activation barrier for conversion to flipamer ‘b’ being 9 kcal/mol (see Figure 7). The flipamers of the  $\text{PPh}_3$ -substituted derivative  $[\mathbf{4e}]^+$  are almost isoenergetic: flipamer ‘b’ is favored by 0.2 kcal/mol, the barrier being 10.5 kcal/mol. The calculated barriers are comparable to those reported for diiron propane-dithiolates (*vide supra*) and are consistent with the observation of two species by EPR spectroscopy. Of course, such a treatment is not applicable for the ethanedithiolate complex  $[\mathbf{2}]^+$ , the EPR spectrum of which can be modeled using a single conformer.

The calculated atomic spin densities show that the majority of the unpaired spin ( $0.7\text{--}0.9 e^-$ ) resides on the Fe atom, with the Ni center only carrying  $\sim 0.1 e^-$  (Table 3). According to these calculations, the conformation of the  $\text{pdt}$  ring has little influence on the spin density distribution and thus on the

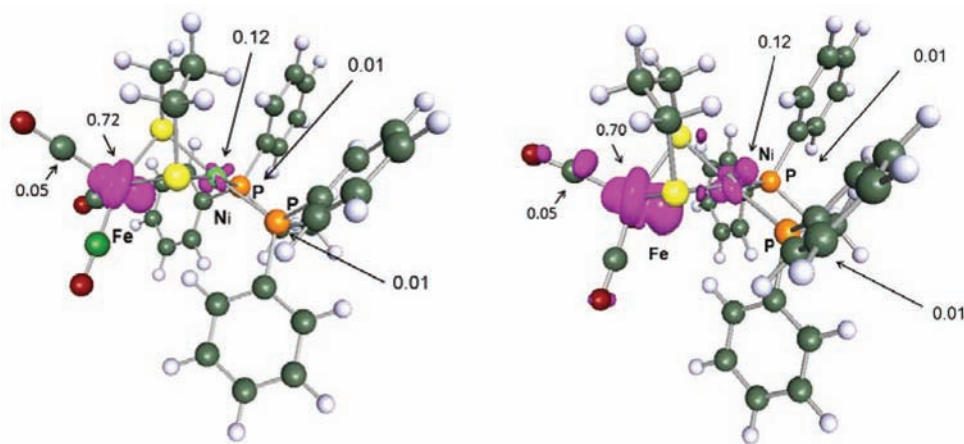


**Figure 7.** Isocontour plots of the unpaired spin density distribution (violet) at  $0.005 e^-/a_0^3$  for the two conformers of  $[\mathbf{1}]^+$ . The central methylene of the  $\text{pdt}^{2-}$  ligand can be oriented toward Ni (left, conformer a) or Fe (right, conformer b). Unpaired atomic spin densities are given for selected nuclei.



**Table 3. Calculated Atomic Spin Populations (BP/TZVP) for Complexes [1]<sup>+</sup>, [2]<sup>+</sup>, [3]<sup>+</sup>, [4a]<sup>+</sup>, and [4e]<sup>+</sup>. The superscripts <sup>a</sup> and <sup>b</sup> refer to the conformations of the pdt-chelate ring (Figure 7)**

BP86/TZVP	$\rho(\text{Fe})$	$\rho(\text{Ni})$	$\rho(\text{P}_{\text{dppe}})$	$\rho(\text{apical})$ C/P
[1] <sup>+</sup> <sup>a</sup>	0.72	0.12	0.01, 0.01	0.05
[1] <sup>+</sup> <sup>b</sup>	0.70	0.12	0.01, 0.01	0.05
[2] <sup>+</sup>	0.72	0.12	0.01, 0.01	0.05
[3] <sup>+</sup> <sup>a</sup>	0.71	0.15	0.01, 0.01	0.05
[3] <sup>+</sup> <sup>b</sup>	0.70	0.13	0.01, 0.01	0.06
[4a] <sup>+</sup> <sup>a</sup>	0.71	0.13	0.01, 0.02	0.05
[4a] <sup>+</sup> <sup>b</sup>	0.74	0.11	0.01, 0.01	0.05

hyperfine interactions. The <sup>31</sup>P nuclei of the bidentate dppe and dcpe ligands give rise to only small hyperfine interactions with isotropic components each between  $-4$  and  $-15$  MHz.

In complexes of type [(diphosphine)Ni(dithiolate)Fe(CO)<sub>2</sub>L]<sup>+</sup>, the apical ligand on the Fe atom can acquire about 5% of the unpaired spin density. For the tricarbonyl cations, this delocalization results in an almost isotropic <sup>13</sup>C hyperfine interaction of +69 to +76 MHz for [1]<sup>+</sup> and [2]<sup>+</sup>, respectively, with a smaller dipolar contribution ( $-5$ ,  $-3$ ,  $+8$  MHz). The hyperfine couplings to the other two <sup>13</sup>CO ligands are significantly smaller ( $-16$ ,  $-17$  MHz) and cannot be resolved in the experimental EPR spectra. In [4e]<sup>+</sup>, there exists a large isotropic hyperfine interaction (+178 and +204 MHz for the two conformers) with the <sup>31</sup>PPh<sub>3</sub> ligand in addition to a small dipolar component ( $-18$ ,  $-16$ ,  $+34$  MHz).

**Mössbauer Spectra.** The neutral complex **1** and the mixed-valence species [4e]BF<sub>4</sub>, [4h]BF<sub>4</sub>, and [4i]BF<sub>4</sub> were studied by Mössbauer spectroscopy. At 6 K and 0.05 T applied field, **1** exhibited a quadrupole doublet ( $\delta = 0.04$  mm/s and  $\Delta E_{\text{Q}} = 0.68$  mm/s), consistent with a diamagnetic complex containing low-spin Fe(I). Under similar conditions, analysis of the diiron(I) species (CO)<sub>3</sub>Fe-(pdt)Fe(CO)<sub>3</sub> yielded the parameters  $\delta = 0.04$  mm/s and  $\Delta E_{\text{Q}} = 0.77$  mm/s (Figure S52, Supporting Information). Similar values have been reported for the related complexes (CO)<sub>3</sub>Fe(SCH<sub>2</sub>O-CH<sub>2</sub>S)(CO)<sub>3</sub><sup>35</sup> and (CO)<sub>3</sub>Fe(SCH<sub>2</sub>Si(CH<sub>3</sub>)<sub>2</sub>CH<sub>2</sub>S)(CO)<sub>3</sub>.<sup>36</sup> These data further highlight the parallels between these two low-spin Fe(I) metal–metal bonded derivatives.

Surprisingly, the one-electron oxidized  $S = 1/2$  complexes [4e]BF<sub>4</sub>, [4h]BF<sub>4</sub>, and [4i]BF<sub>4</sub> in the solid state also exhibited quadrupole doublets at 6 K and 0.05 T. The spectra appeared to be inconsistent with the EPR and DFT studies (*vide supra*), which indicated unpaired spin density on these complexes, primarily on the Fe (Figure 8). In such cases, it was expected

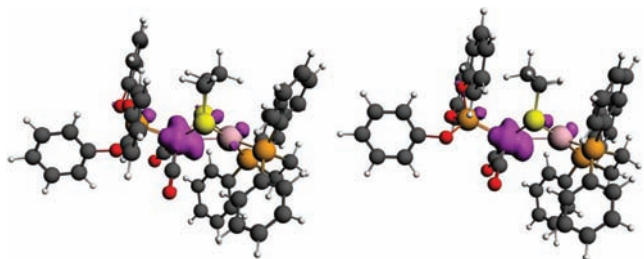


**Figure 8.** Isocontour plots of the unpaired spin density distribution (violet) at  $0.005 e^-/a_0^3$  for the two conformers of [4a]<sup>+</sup>. The central methylene of the pdt<sup>2-</sup> ligand can be oriented toward Ni (left, conformer a) or Fe (right, conformer b).

that paramagnetic hyperfine structure would be observed under the experimental conditions employed.

It was reasoned that the apparent inconsistency could be due to intermolecular spin–spin interactions. Accordingly, [4e]BF<sub>4</sub> was studied at 4.3 K in a strong applied magnetic field (6 T), where these interactions would be less apparent. Indeed, the high-field data indicated the presence of magnetic hyperfine interactions, which prompted us to examine a frozen solution of [4e]BF<sub>4</sub> (5 mM, CH<sub>2</sub>Cl<sub>2</sub>/PhMe, 1:2). At 6 K and 0.05 T applied field, the Mössbauer spectrum of the solution indicated the presence of magnetic hyperfine interactions. Such low concentrations circumvented spin–spin interactions but resulted in noisy spectra. Analysis of a more concentrated sample (40 mM) afforded a similar low-field, low-temperature spectrum but with higher S/N (Figure S53, Supporting Information). Indeed, data collected at applied fields of 4 and 6 T were, apart from the poorer S/N, indistinguishable from those of solid [4e]BF<sub>4</sub>. The low field spectrum of this frozen solution and the high-temperature, high-field data of the solid sample could be simulated with an  $S = 1/2$  Hamiltonian (Figure 9, parameters in

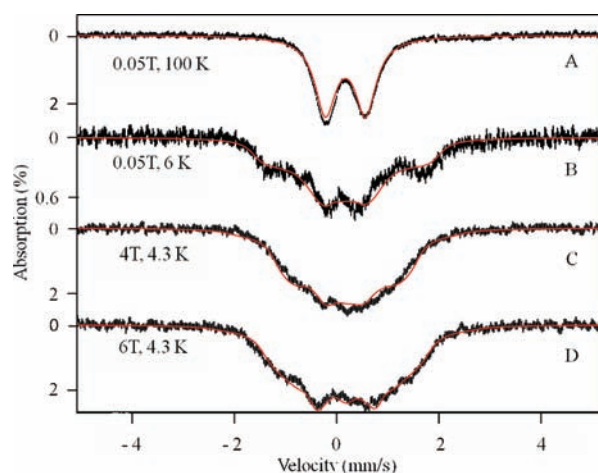
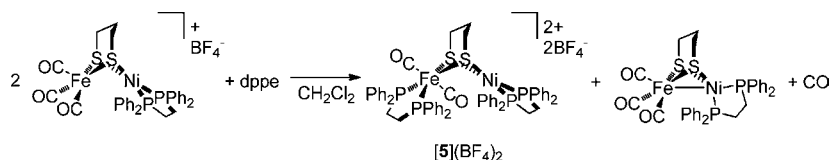


**Figure 9.** Mössbauer spectra of [4e]BF<sub>4</sub> recorded at the applied fields and temperatures indicated. Spectra A, C, and D were obtained on a solid sample, while spectrum B was obtained on a 40 mM frozen solution. The magnetic field was parallel to the  $\gamma$  beam for spectra A and B and transverse to the  $\gamma$  beam for spectra C and D. The solid line through the data is a simulation using an  $S = 1/2$  Hamiltonian with the parameters  $\delta = 0.18$  mm/s,  $\Delta E_{\text{Q}} = 0.79$  mm/s,  $\eta = 0.7$ ,  $A/(g\beta_n) = (+6.2, -5.5, -28.1)$  KG,  $\beta_{\text{eff}} = 45^\circ$ , and  $\gamma_{\text{eff}} = 90^\circ$ .

caption). The DFT calculated Mössbauer parameters of  $\eta = 0.8$  and a NQCC of 11 MHz agree well with those measured. The <sup>57</sup>Fe hyperfine tensor for [4e]BF<sub>4</sub> has a small isotropic component,  $A_{\text{iso}} = (A_x + A_y + A_z)/3 = -9.1$  MHz and significant anisotropy. The calculated <sup>57</sup>Fe isotropic hyperfine coupling parameters ( $A_{\text{iso}} = -4$  MHz for SR UKS ZORA B3LYP/TZP and  $A_{\text{iso}} = -1.5$  MHz for SR UKS ZORA BP/TZP) and larger anisotropic hyperfine tensors (SR UKS B3LYP/TZP ( $-22$ ,  $-10$ ,  $+32$ ) MHz and SR UKS BP/TZP ( $-18$ ,  $-9$ ,  $+27$ ) MHz) are in good agreement with those measured.

**Disproportionation Reactions.** Interaction of [1]<sup>+</sup> with small basic phosphine ligands results in complicated mixtures. For example, addition of [1]<sup>+</sup> to excess PBu<sub>3</sub> in CH<sub>2</sub>Cl<sub>2</sub> induces a “disproportionation” reaction affording **1** and a product formulated as [(dppe)Ni(pdt)Fe(CO)<sub>2</sub>(PBu<sub>3</sub>)<sub>2</sub>](BF<sub>4</sub>)<sub>2</sub>. Precipitation of the latter compound allowed for its identification according to ESI–MS ( $m/z$  1166.1 [M – BF<sub>4</sub>]<sup>+</sup>, 539.5 [M – 2BF<sub>4</sub>]<sup>2+</sup>) and <sup>31</sup>P NMR (60 (dppe), 28 (PBu<sub>3</sub>) ppm) data. A strong  $\nu_{\text{CO}}$  band could be observed at  $1965 \text{ cm}^{-1}$ , with a

Scheme 6



weaker one at 2037 cm<sup>-1</sup>. Along with the NMR data, these data indicate the presence of a Fe(II)(CO)<sub>2</sub>(PBu<sub>3</sub>)<sub>2</sub> fragment in which the CO ligands are mutually trans, although other isomers could be present. Similar products were observed when PMe<sub>3</sub> ( $\nu_{\text{CO}}$  1971 cm<sup>-1</sup>,  $m/z$  913.5 [M - BF<sub>4</sub><sup>-</sup>]<sup>+</sup>, 413.6 [M - 2BF<sub>4</sub><sup>-</sup>]<sup>2+</sup>) and PMe<sub>2</sub>Ph ( $\nu_{\text{CO}}$  1971 cm<sup>-1</sup>,  $m/z$  1037.5 [M - BF<sub>4</sub><sup>-</sup>]<sup>+</sup>, 475.3 [M - 2BF<sub>4</sub><sup>-</sup>]<sup>2+</sup>) were employed in place of PBu<sub>3</sub>. Overall, these data suggest that a disproportionation-type reaction is triggered when a sufficiently small pair of ligands bind Fe.

More tractable products of disproportionation were obtained when the diphosphine dppe was used. At room temperature, a rapid reaction was indicated by IR spectroscopy; the products are **1** and the new salt formulated as [(dppe)Ni(pdt)Fe(CO)<sub>2</sub>(dppe)](BF<sub>4</sub>)<sub>2</sub> ([5](BF<sub>4</sub>)<sub>2</sub>) (Scheme 6).

This compound can be prepared in good yield by treatment of a CH<sub>2</sub>Cl<sub>2</sub> solution of **1** and FcBF<sub>4</sub> (2 equiv) with dppe. On the basis of its <sup>1</sup>H and <sup>31</sup>P NMR spectra, [5]<sup>2+</sup> is diamagnetic and symmetrical in CD<sub>2</sub>Cl<sub>2</sub> solution. Further evidence supporting the proposed structure could be obtained by ESI-MS, which allowed for the detection of ions at  $m/z$  1158.7 and 536.1, assigned to {[5]BF<sub>4</sub>}<sup>+</sup> and [5]<sup>2+</sup>, respectively.

**Structure of [(dppe)Ni(pdt)Fe(CO)<sub>2</sub>(dppe)](BF<sub>4</sub>)<sub>2</sub>.** The solid state structure of [5]<sup>2+</sup> was established by X-ray crystallography (Figure 10).

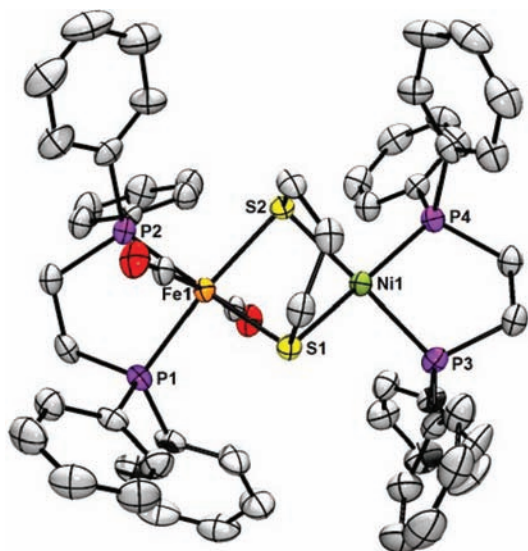


**Figure 10.** ORTEP of [5](BF<sub>4</sub>)<sub>2</sub>·4CH<sub>2</sub>Cl<sub>2</sub> with ellipsoids drawn at the 50% probability level. The H atoms, disordered BF<sub>4</sub><sup>-</sup> anions, and four CH<sub>2</sub>Cl<sub>2</sub> solvate molecules are omitted for clarity. Selected distances (Å): Ni1–Fe1, 2.818; Fe1–P1, 2.254; Fe1–P2, 2.262; Fe1–C27, 1.800; Fe1–C28, 1.817; Fe1–S1, 2.325; Fe1–S2, 2.334; Ni1–S1, 2.219; Ni1–S2, 2.253; Ni1–P3, 2.186; Ni1–P4, 2.180.

As expected, the complex dication features a pdt<sup>2-</sup> ligand bridging the Ni and Fe centers, which exist in square planar and octahedral ligand environments, respectively. These coordination geometries, and a Ni–Fe distance of 3.203 Å, are reflective

of a Ni(II)Fe(II) complex lacking a metal–metal bond. The Fe–C distances (1.800, 1.817 Å) are similar, and these solid-state data are corroborated by the IR solution spectrum, which features a single CO band (1975 cm<sup>-1</sup>), consistent with the presence of two *trans* CO ligands. Indeed, the complex is roughly symmetric, as evidenced by the two Fe–S (2.325, 2.334 Å), Ni–P (2.180, 2.186 Å), and Ni–S (2.219, 2.253 Å) bonds of similar pairwise lengths. These are comparable to the average Ni–P (2.176 Å) and Ni–S (2.222 Å) distances in the related dinickel(II) complex {(pdt)[Ni(dppe)]<sub>2</sub>}(BF<sub>4</sub>)<sub>2</sub>.<sup>37</sup> The product resembles [(dppe)Ni(pdt)Fe(CO)<sub>2</sub>(CN)<sub>2</sub>]<sup>18</sup> and might be compared with the 34e<sup>-</sup> Ni(II)Fe(II) core present in the Ni-SCO state of [NiFe]-H<sub>2</sub>ase.

## DISCUSSION

Oxidation of Ni(I)Fe(I) dithiolates affords mixed-valence derivatives, which are described as Ni(II)Fe(I) species. Several lines of evidence support this assignment: (i) crystallographic analysis shows that Fe–C bond lengths are unaffected by oxidation of the Ni(I)Fe(I) precursor whereas the Ni coordination geometry changes from being tetrahedral to square planar, (ii) in the EPR spectra of the cations, hyperfine coupling is observed with <sup>13</sup>CO (on Fe) but not the diphosphine (on Ni), and (iii) the Mössbauer parameters observed are similar to other Fe(I) sites. Additionally, as has recently been described, the potentials for the oxidation of Ni(dppe) derivative **1** vs. the Ni(dcpe) derivative **3** differ strongly ( $E_{1/2} = -0.54$  and  $-0.84$  V vs Fc/Fc<sup>+</sup>, respectively).<sup>23</sup>

In view of the electron-rich Fe(CN)<sub>2</sub>(CO) fragment present in the [NiFe]-H<sub>2</sub>ase active site, it was of interest to further modify the tricarbonyl cations by introducing donor ligands. It was anticipated that the displacement of one or more of the CO ligands in [1]<sup>+</sup> with stronger  $\sigma$ -donors would stabilize oxidation states matching those of the Ni-L state of the enzyme (Ni(I)Fe(II)). For example, ENDOR measurements on the Ni-A state revealed a small  $A(^{57}\text{Fe})$  of 1 MHz, and no hyperfine could be resolved for the enzyme in the Ni-B and Ni-C states.<sup>38</sup> However, the substituted complexes [4a–j]<sup>+</sup> also appear to be Ni(II)Fe(I) derivatives in which the monodentate P-donor ligands occupy the apical Fe coordination site. Donor atoms at this site are proposed to interact strongly with the Fe-centered SOMO, as indicated by the observation of strong hyperfine coupling to only a single <sup>13</sup>CO center in [1]<sup>+</sup>. This trend is supported by considering the minimal effect that <sup>13</sup>CO labeling has on the EPR spectrum of [4e]<sup>+</sup>, suggesting that the (basal) <sup>13</sup>CO ligands in this complex are only weakly coupled to the SOMO.

The substituted derivatives [4a–j]<sup>+</sup> are expected to be approximately isostructural to one another, given the correlation between  $\nu_{\text{CO}}$  and TEP values for the complexes. The apical location of the P-donor ligands in these salts contrasts with the structure of the hydride [(dppe)Ni(pdt)( $\mu$ -H)Fe(CO)<sub>2</sub>PPh<sub>3</sub>]<sup>+</sup>, in which PPh<sub>3</sub> occupies a basal coordination site.<sup>21</sup> The latter conformation is undoubtedly stabilized by the mutually *trans* arrangement of the H<sup>-</sup> (strong  $\sigma$ -donor) and CO ( $\pi$ -acceptor)



ligands. The stereochemistry at Fe in the new complexes also differs from the enzyme, in which the two strongly  $\sigma$ -donating CN<sup>-</sup> ligands occupy the *basal* sites.

Using <sup>13</sup>CO labeling, we confirmed that both **1** and [1]BF<sub>4</sub> rapidly exchange with CO, which may be relevant to the well-known observation that exogenous CO inhibits [NiFe]-H<sub>2</sub>ase. Binding of CO to Ni-SI<sub>a</sub> affords the EPR-silent Ni-SCO and Ni-SCO<sub>red</sub> states,<sup>39</sup> while Ni-L reacts with CO to give the Ni-CO state.<sup>40</sup> The latter state is paramagnetic ( $S = 1/2$ ) and features CO coordinated to Ni(I).<sup>41</sup> Although no analogous CO adduct of [1]BF<sub>4</sub> was observed in our work, short-lived CO adducts would explain the facility by which these cations exchange with CO. It appears likely that the exogenous CO ligand would bind the Fe center; a similar adduct with tertiary phosphine ligands would be an intermediate in the conversion of [1]BF<sub>4</sub> to [4a-j]BF<sub>4</sub>.

There are notable differences between the spectroscopy of the mixed-valence complexes discussed here and data reported for the Ni-L state of [NiFe]-H<sub>2</sub>ase.<sup>38</sup> Solution IR data for the mixed-valence complexes suggest that the Fe center in each of these derivatives is still electron-poor relative to the enzyme ( $\nu_{\text{CO}} = 1911 \text{ cm}^{-1}$  for Ni-L state of *D. vulgaris* Miyazaki F).<sup>42</sup> More significantly, the spin in this state is predominantly localized in the Ni  $d(x^2 - y^2)$  and  $d(z^2)$  orbitals, with the  $g$ -values obtained being 2.298, 2.116, and 2.043.<sup>43</sup> These  $g$ -values are considerably larger than those found for [2]BF<sub>4</sub> (2.053, 2.054, 2.010), in which the spin likely resides on the Fe center. It appears that the incorporation of monophosphines into [1]<sup>+</sup> is insufficient to reverse the Ni(II)Fe(I) oxidation state assignment of [1]<sup>+</sup>. In fact, instead of resembling Ni-L, the data for the new complexes are closer to those for the [2Fe]<sub>H</sub> component in the H<sub>ox</sub> state of [FeFe]-H<sub>2</sub>ase. In the enzyme isolated from *C. pasteurianum*, this Fe(I)Fe(II) cluster exhibited an EPR signal with  $g = 2.097, 2.039, 1.999$ .<sup>44</sup>

Mössbauer spectra of the diamagnetic Ni(I)Fe(I) complex **1** and the closely related one-electron-oxidized  $S = 1/2$  species were collected to give evidence for the description of the latter as Ni(II)Fe(I) species, given that a more delocalized description might have been possible. Most useful in this analysis were the Fe isomer shifts  $\delta$ , as well as the magnitude and anisotropy of the  $A$ -tensors. The  $\delta$  value was found to be slightly greater for [4e]BF<sub>4</sub> relative to **1**, a fact that could suggest the Fe center in the former to be oxidized relative to the Fe(I) center in the latter. However, the isomer shift could also reflect differences in coordination environment, given that a CO ligand is substituted for PPh<sub>3</sub> in [4e]BF<sub>4</sub>. Low-spin Fe(II) can be ruled out given that a very low Fe-centered spin density and  $A$ -values would be expected in such a case. The  $A$ -tensor of [4e]BF<sub>4</sub> is modest but large enough to support an Fe(I) assignment. Popescu and co-workers also required a relatively small  $A_{\text{iso}}$  value (9.5 MHz) to simulate Mössbauer spectra of the [2Fe]<sub>H</sub> component in the H<sub>ox</sub>-CO state of [FeFe]-H<sub>2</sub>ase from *Clostridium pasteurianum*,<sup>45</sup> although the magnetic hyperfine tensors used were isotropic unlike those employed to simulate spectra of [4e]BF<sub>4</sub>. From DFT studies using the ADF program, Brunold and co-workers calculated highly anisotropic  $A$  values, including +11, -1, and -27.5 MHz, for the Fe(I) center in H<sub>ox</sub>.<sup>46</sup> These values are similar in both sign and magnitude to those used in our simulation, indicating that the <sup>57</sup>Fe hyperfine tensor for [4e]BF<sub>4</sub> is best explained by a low-spin Fe(I) center. The assignment is also corroborated by our DFT calculations, which gave an unpaired spin density of  $0.85e^-$  at the Fe atom of [4e]BF<sub>4</sub>. The increase of  $\delta$ , relative to that of **1**, suggests some

degree of oxidation, but other low-spin Fe(I) centers with similar  $\delta$  (0.12 mm/s) have been reported.<sup>47</sup> The low-spin Fe(I)Fe(II) cluster in H<sub>ox</sub> from *C. pasteurianum* has  $0.1 < \delta < 0.3 \text{ mm/s}$ ; in the H<sub>ox</sub>-CO state from *D. vulgaris*, it has  $\delta_{1,2} = 0.13, 0.17 \text{ mm/s}$ ,<sup>45,48</sup> similar to the  $\delta$  value associated with the Fe(I) in [4e]BF<sub>4</sub>.

## SUMMARY

The first examples of mixed-valence ( $S = 1/2$ ) nickel-iron dithiolates have been prepared. Complexes of the type [(dxpe)-Ni(xdt)Fe(CO)<sub>2</sub>L]<sup>+</sup> are characterized as Ni(II)Fe(I) mixed-valence species on the basis of structural and spectroscopic data. The Ni(II)Fe(I) assignment contrasts the Ni(I)Fe(II) core present in the Ni-L state of [NiFe]-H<sub>2</sub>ase and is perhaps more related to the Fe(I)Fe(II) fragment in the H<sub>ox</sub> state of [FeFe]-H<sub>2</sub>ase. The crystallographic results highlight the large geometric changes upon oxidation of the Ni(I)Fe(I) precursor, suggesting that stabilization of Ni(I)Fe(II) complexes may require not just changes in the terminal ligands, but also greater control of the nickel coordination sphere to better match the seesaw geometry observed for the enzyme.

## EXPERIMENTAL SECTION

Unless otherwise stated, all chemicals were purchased from commercial sources and used as received. PMe<sub>3</sub> was distilled from CaH<sub>2</sub>. The compounds **1**,<sup>22</sup> **2**, **3**,<sup>23</sup> and PPh<sub>2</sub>(*o*-C<sub>6</sub>H<sub>4</sub>OCH<sub>2</sub>OCH<sub>3</sub>)<sup>49</sup> were prepared according to the literature methods.

All reactions were conducted in an MBraun glovebox equipped with a solvent purification system; the concentrations of O<sub>2</sub> and H<sub>2</sub>O in the N<sub>2</sub> atmosphere were less than 1 ppm. The mixed-valence complexes were stored at -28 °C. IR spectra of complexes (in CH<sub>2</sub>Cl<sub>2</sub>) were recorded on a Perkin-Elmer Spectrum 100 FTIR spectrometer. EPR spectra of complexes (~1 mM in CH<sub>2</sub>Cl<sub>2</sub>/PhMe, 1:1) were recorded on a Varian E-line 12" Century Series X-band CW spectrometer. ESI-MS data were acquired using a Waters Micromass Quattro II spectrometer. Analytical data were acquired using an Exeter Analytical CE-440 elemental analyzer. UV-vis data were acquired on a Varian Cary 50 Bio spectrophotometer. NMR spectra were recorded at room temperature on a Varian Unity 500 spectrometer. <sup>31</sup>P{<sup>1</sup>H} spectra were collected at 500 MHz and chemical shifts are referenced to external 85% H<sub>3</sub>PO<sub>4</sub>. Crystallographic data were collected using a Siemens SMART diffractometer equipped with a Mo K $\alpha$  source ( $\lambda = 0.71073 \text{ \AA}$ ) and an Apex II detector. Mössbauer spectra were collected for samples either suspended in mineral oil or dissolved in CH<sub>2</sub>Cl<sub>2</sub>/PhMe (1:2). Of the instruments used (MS4 WRC and 12CNDT-6T spectrometers, SEE Co., Edina MN), the former allowed data collection at 6 K with 0.05 T field applied parallel to the  $\gamma$  rays, while the latter gave data at 4.3 K with perpendicular fields as high as 6 T. Spectra were analyzed with WMOSS software. Isomer shifts are quoted relative to  $\alpha$ -iron at 298 K.

[(dppe)Ni(pdt)Fe(<sup>13</sup>CO)<sub>3</sub>] (**1**). Compound **1** (21.1 mg, 30.0  $\mu\text{mol}$ ) was dissolved in CH<sub>2</sub>Cl<sub>2</sub> (5 mL), and the solution was frozen with liquid N<sub>2</sub>. The reaction vessel was evacuated; the solution was placed under <sup>13</sup>CO (1 atm) and warmed to room temperature. The mixture was briefly agitated, allowed to stand for 2 h, and evaporated to dryness to afford the product as a green powder (quant.).

FT-IR:  $\nu_{\text{CO}} = 1982, 1913 \text{ cm}^{-1}$ . <sup>13</sup>C NMR (126 MHz) 209.3 ppm. <sup>31</sup>P NMR (202 MHz) 63.5 ppm. Anal. Calcd for C<sub>29</sub><sup>13</sup>C<sub>3</sub>H<sub>30</sub>FeNiO<sub>3</sub>·P<sub>2</sub>S<sub>2</sub>·0.5CH<sub>2</sub>Cl<sub>2</sub>: C, 52.14; H, 4.17; N, 0.00. Found: C, 52.41; H, 4.36; N, 0.00.

[(dppe)Ni(pdt)Fe(CO)<sub>3</sub>]BF<sub>4</sub> ([1]BF<sub>4</sub>). Compound **1** (14.1 mg, 20.0  $\mu\text{mol}$ ) and FcBF<sub>4</sub> (5.5 mg, 20.0  $\mu\text{mol}$ ) were dissolved in CH<sub>2</sub>Cl<sub>2</sub> (2 mL) with rapid stirring. After 1 min, pentane (-28 °C, 15 mL) was added, and the mixture was allowed to stand at -28 °C for 10 min. A solid was isolated by filtration, washed with pentane (-28 °C, 2  $\times$  2 mL), and dried briefly to afford the product as a brown powder (12.0 mg, 15.2  $\mu\text{mol}$ , 76%).

FT-IR:  $\nu_{\text{CO}} = 2057, 1986 \text{ cm}^{-1}$ . ESI-MS:  $m/z$  702.1  $[\text{M} - \text{BF}_4]^{-}$ . Anal. Calcd for  $\text{C}_{32}\text{H}_{30}\text{BF}_4\text{FeNiO}_3\text{P}_3\text{S}_2 \cdot 0.5\text{SCH}_2\text{Cl}_2$ : C, 46.89; H, 3.75; N, 0.00. Found: C, 46.73; H, 3.85; N, 0.28.

**[(dpe)Ni(pdt)Fe(CO)<sub>3</sub>PF<sub>6</sub>] ([1]PF<sub>6</sub>)**. This salt was prepared analogously to **[1]BF<sub>4</sub>**, using **FcPF<sub>6</sub>** in place of **FcBF<sub>4</sub>**. Yield: 78%, brown powder.

FT-IR:  $\nu_{\text{CO}} = 2057, 1986 \text{ cm}^{-1}$ . Anal. Calcd for  $\text{C}_{32}\text{H}_{30}\text{F}_6\text{FeNiO}_3\text{P}_3\text{S}_2 \cdot 0.25\text{SCH}_2\text{Cl}_2$ : C, 44.55; H, 3.54; N, 0.00. Found: C, 44.51; H, 3.61; N, 0.32.

**[(dpe)Ni(pdt)Fe(<sup>13</sup>CO)<sub>3</sub>BF<sub>4</sub>] ([1']BF<sub>4</sub>)**. This salt was prepared analogously to **[1]BF<sub>4</sub>**, using **1'** as the precursor. Yield: 78%, yellow-brown powder.

FT-IR:  $\nu_{\text{CO}} = 2009, 1941 \text{ cm}^{-1}$ . Anal. Calcd for  $\text{C}_{32}^{13}\text{C}_3\text{H}_{30}\text{BF}_4\text{FeNiO}_3\text{P}_3\text{S}_2 \cdot 0.75\text{SCH}_2\text{Cl}_2$ : C, 45.91; H, 3.71; N, 0.00. Found: C, 45.96; H, 3.80; N, 0.00.

**[1]BARF<sub>4</sub>**. Compound **1** (7.0 mg, 10  $\mu\text{mol}$ ) and **FcBARF<sub>4</sub>** (10.5 mg, 10  $\mu\text{mol}$ ) were dissolved in  $\text{CH}_2\text{Cl}_2$  (1 mL) with rapid stirring. The deep brown solution was used *in situ* for reactivity studies.

FT-IR:  $\nu_{\text{CO}} = 2057, 1986 \text{ cm}^{-1}$ .

**[(dpe)Ni(edt)Fe(CO)<sub>3</sub>BF<sub>4</sub>] ([2]BF<sub>4</sub>)**. Compound **2** (6.9 mg, 10.0  $\mu\text{mol}$ ) and **FcBF<sub>4</sub>** (2.7 mg, 10.0  $\mu\text{mol}$ ) were dissolved in  $\text{CH}_2\text{Cl}_2$  (1 mL) with rapid stirring. The deep brown solution was used for *in situ* EPR and IR analyses, the latter indicating that significant amounts of the diamagnetic species **2** and **[2H]BF<sub>4</sub>** were present in the crude mixture. The solution was diluted with PhMe for the EPR analysis.

FT-IR:  $\nu_{\text{CO}} = 2059, 1988 \text{ cm}^{-1}$ . ESI-MS:  $m/z$  688.1  $[\text{M} - \text{BF}_4]^{-}$ .

**[(dcpe)Ni(pdt)Fe(CO)<sub>3</sub>BF<sub>4</sub>] ([3]BF<sub>4</sub>)**. This salt was prepared analogously to **[1]BF<sub>4</sub>**, using **3** as the precursor. Yield: 78%, brown powder.

FT-IR:  $\nu_{\text{CO}} = 2054, 1982 \text{ cm}^{-1}$ . ESI-MS:  $m/z$  726.3  $[\text{M} - \text{BF}_4]^{-}$ . Anal. Calcd for  $\text{C}_{32}\text{H}_{34}\text{BF}_4\text{FeNiO}_3\text{P}_3\text{S}_2 \cdot 2.25\text{SCH}_2\text{Cl}_2$ : C, 40.92; H, 5.87; N, 0.00. Found: C, 40.90; H, 5.82; N, 0.00.

Brown plate-like single crystals of **[3]BF<sub>4</sub>·2CH<sub>2</sub>Cl<sub>2</sub>** were grown by layering a concentrated  $\text{CH}_2\text{Cl}_2$  solution with pentane and allowing the mixture to stand at  $-28 \text{ }^\circ\text{C}$ . One crystal ( $0.544 \times 0.295 \times 0.062 \text{ mm}^3$ ) was subjected to X-ray diffraction at 193 K. Its space group was determined to be monoclinic  $P2_1/c$  with cell parameters:  $a = 16.680 \text{ \AA}$ ,  $b = 15.715 \text{ \AA}$ ,  $c = 17.193 \text{ \AA}$ ,  $\alpha = 90.00^\circ$ ,  $\beta = 92.84^\circ$ ,  $\gamma = 90.00^\circ$ . Integration of 3591 reflections and solution by direct methods using SHELXTL V6.12<sup>50,51</sup> afforded a model with  $R1 = 0.0527$  and  $wR2 = 0.1228$ .

**Phosphine-Substituted Derivatives ([4a–j]BF<sub>4</sub>)**. Compound **1** (14.1 mg, 20  $\mu\text{mol}$ ) and **FcBF<sub>4</sub>** (5.5 mg, 20  $\mu\text{mol}$ ) were dissolved in  $\text{CH}_2\text{Cl}_2$  (2 mL) with rapid stirring. After 1 min, the solution was added dropwise to the appropriate phosphine (200  $\mu\text{mol}$ ) in  $\text{CH}_2\text{Cl}_2$  (0.5 mL). The solution was stirred for another 0.5 min, pentane ( $-28 \text{ }^\circ\text{C}$ , 15 mL) was added, and the mixture was allowed to stand at  $-28 \text{ }^\circ\text{C}$  for 1 h. The solids were isolated by filtration, washed with pentane ( $-28 \text{ }^\circ\text{C}$ ,  $2 \times 2 \text{ mL}$ ), and dried briefly to afford the respective phosphine complexes. The <sup>13</sup>CO derivatives were prepared analogously using **1'** as the precursor.

**[(dpe)Ni(pdt)Fe(CO)<sub>2</sub>P(OPh)<sub>3</sub>BF<sub>4</sub>] ([4a]BF<sub>4</sub>)**. Yield: 78%, yellow-brown powder. ESI-MS:  $m/z$  983.9  $[\text{M} - \text{BF}_4]^{-}$ . Anal. Calcd for  $\text{C}_{49}\text{H}_{45}\text{BF}_4\text{FeNiO}_3\text{P}_3\text{S}_2 \cdot 0.5\text{SCH}_2\text{Cl}_2$ : C, 53.33; H, 4.16; N, 0.00. Found: C, 53.41; H, 4.11; N, 0.31.

**[(dpe)Ni(pdt)Fe(<sup>13</sup>CO)<sub>2</sub>P(OPh)<sub>3</sub>BF<sub>4</sub>] ([4a']BF<sub>4</sub>)**. Yield: 70%, yellow-brown powder. ESI-MS:  $m/z$  986.0  $[\text{M} - \text{BF}_4]^{-}$ . Anal. Calcd for  $\text{C}_{47}^{13}\text{C}_2\text{H}_{45}\text{BF}_4\text{FeNiO}_3\text{P}_3\text{S}_2 \cdot 0.5\text{SCH}_2\text{Cl}_2$ : C, 53.24; H, 4.15; N, 0.00. Found: C, 52.97; H, 4.15; N, 0.00.

**[(dpe)Ni(pdt)Fe(CO)<sub>2</sub>P(p-C<sub>6</sub>H<sub>4</sub>Cl)<sub>3</sub>BF<sub>4</sub>] ([4b]BF<sub>4</sub>)**. Yield: 87%, yellow-brown powder. ESI-MS:  $m/z$  1040.0  $[\text{M} - \text{BF}_4]^{-}$ . Anal. Calcd for  $\text{C}_{49}\text{H}_{42}\text{BF}_4\text{FeNiO}_3\text{P}_3\text{S}_2 \cdot 0.67\text{CH}_2\text{Cl}_2$ : C, 50.36; H, 3.69; N, 0.00. Found: C, 50.49; H, 3.77; N, 0.01.

**[(dpe)Ni(pdt)Fe(CO)<sub>2</sub>PPh<sub>2</sub>(2-py)]BF<sub>4</sub>] ([4c]BF<sub>4</sub>)**. Yield: 80%, yellow-brown powder. ESI-MS:  $m/z$  937.1  $[\text{M} - \text{BF}_4]^{-}$ , 908.0  $[\text{M} - \text{CO} - \text{BF}_4]^{-}$ . Anal. Calcd for  $\text{C}_{48}\text{H}_{44}\text{BF}_4\text{FeNiO}_2\text{P}_3\text{S}_2 \cdot 0.25\text{SCH}_2\text{Cl}_2$ : C, 55.38; H, 4.29; N, 1.34. Found: C, 55.30; H, 4.28; N, 1.58.

**[(dpe)Ni(pdt)Fe(CO)<sub>2</sub>PPh<sub>2</sub>(OEt)]BF<sub>4</sub>] ([4d]BF<sub>4</sub>)**. Yield: 81%, yellow-brown powder. ESI-MS:  $m/z$  904.0  $[\text{M} - \text{BF}_4]^{-}$ , 567.2  $[\text{M} +$

$\text{PPh}_2(\text{OEt}) - \text{BF}_4]^{-2+}$ . Anal. Calcd for  $\text{C}_{45}\text{H}_{45}\text{BF}_4\text{FeNiO}_3\text{P}_3\text{S}_2 \cdot 0.25\text{SCH}_2\text{Cl}_2$ : C, 53.63; H, 4.53; N, 0.00. Found: C, 53.50; H, 4.74; N, 0.06.

**[(dpe)Ni(pdt)Fe(CO)<sub>2</sub>PPh<sub>3</sub>BF<sub>4</sub>] ([4e]BF<sub>4</sub>)**. Yield: 93%, yellow-brown powder. ESI-MS:  $m/z$  936.3  $[\text{M} - \text{BF}_4]^{-}$ . Anal. Calcd for  $\text{C}_{49}\text{H}_{45}\text{BF}_4\text{FeNiO}_2\text{P}_3\text{S}_2 \cdot 0.75\text{SCH}_2\text{Cl}_2$ : C, 54.92; H, 4.31; N, 0.00. Found: C, 54.70; H, 4.32; N, 0.34.

**[(dpe)Ni(pdt)Fe(<sup>13</sup>CO)<sub>2</sub>PPh<sub>3</sub>BF<sub>4</sub>] ([4e']BF<sub>4</sub>)**. Yield: 73%, yellow-brown powder. ESI-MS:  $m/z$  938.0  $[\text{M} - \text{BF}_4]^{-}$ . Anal. Calcd for  $\text{C}_{47}^{13}\text{C}_2\text{H}_{45}\text{BF}_4\text{FeNiO}_2\text{P}_3\text{S}_2 \cdot 0.75\text{SCH}_2\text{Cl}_2$ : C, 54.82; H, 4.30; N, 0.00. Found: C, 54.70; H, 4.29; N, 0.00.

**[(dpe)Ni(pdt)Fe(CO)<sub>2</sub>PPh<sub>2</sub>(o-C<sub>6</sub>H<sub>4</sub>OMe)]BF<sub>4</sub>] ([4f]BF<sub>4</sub>)**. Yield: 67%, brown powder. ESI-MS:  $m/z$  966.2  $[\text{M} - \text{BF}_4]^{-}$ . Anal. Calcd for  $\text{C}_{50}\text{H}_{47}\text{BF}_4\text{FeNiO}_3\text{P}_3\text{S}_2 \cdot 0.5\text{SCH}_2\text{Cl}_2$ : C, 55.30; H, 4.41; N, 0.00. Found: C, 55.09; H, 4.25; N, 0.38.

**[(dpe)Ni(pdt)Fe(CO)<sub>2</sub>PPh<sub>2</sub>(o-C<sub>6</sub>H<sub>4</sub>OCH<sub>2</sub>OMe)]BF<sub>4</sub>] ([4g]BF<sub>4</sub>)**. Yield: 63%, brown powder. ESI-MS:  $m/z$  996.4  $[\text{M} - \text{BF}_4]^{-}$ . Anal. Calcd for  $\text{C}_{51}\text{H}_{49}\text{BF}_4\text{FeNiO}_4\text{P}_3\text{S}_2 \cdot \text{CH}_2\text{Cl}_2$ : C, 53.41; H, 4.40; N, 0.00. Found: C, 53.44; H, 4.35; N, 0.34.

**[(dpe)Ni(pdt)Fe(CO)<sub>2</sub>P(p-tol)<sub>3</sub>BF<sub>4</sub>] ([4h]BF<sub>4</sub>)**. Yield: 89%, yellow-brown powder. ESI-MS:  $m/z$  978.3  $[\text{M} - \text{BF}_4]^{-}$ . Anal. Calcd for  $\text{C}_{52}\text{H}_{51}\text{BF}_4\text{FeNiO}_3\text{P}_3\text{S}_2 \cdot 0.5\text{SCH}_2\text{Cl}_2$ : C, 56.87; H, 4.73; N, 0.00. Found: C, 56.58; H, 4.63; N, 0.32.

**[(dpe)Ni(pdt)Fe(CO)<sub>2</sub>P(p-C<sub>6</sub>H<sub>4</sub>OMe)<sub>3</sub>BF<sub>4</sub>] ([4i]BF<sub>4</sub>)**. Yield: 96%, yellow-brown powder. ESI-MS:  $m/z$  1026.3  $[\text{M} - \text{BF}_4]^{-}$ . Anal. Calcd for  $\text{C}_{52}\text{H}_{51}\text{BF}_4\text{FeNiO}_3\text{P}_3\text{S}_2 \cdot 0.25\text{SCH}_2\text{Cl}_2$ : C, 55.26; H, 4.57; N, 0.00. Found: C, 55.26; H, 4.75; N, 0.25.

**[(dpe)Ni(pdt)Fe(CO)<sub>2</sub>PMePh<sub>2</sub>]BF<sub>4</sub>] ([4j]BF<sub>4</sub>)**. Yield: 76%, brown powder. ESI-MS:  $m/z$  874.3  $[\text{M} - \text{BF}_4]^{-}$ . Anal. Calcd for  $\text{C}_{44}\text{H}_{43}\text{BF}_4\text{FeNiO}_2\text{P}_3\text{S}_2 \cdot \text{CH}_2\text{Cl}_2$ : C, 51.62; H, 4.33; N, 0.00. Found: C, 51.90; H, 4.35; N, 0.23.

**[(dpe)Ni(pdt)Fe(CO)<sub>2</sub>dpe](BF<sub>4</sub>)<sub>2</sub>] ([5](BF<sub>4</sub>)<sub>2</sub>)**. Compound **1** (14.1 mg, 20  $\mu\text{mol}$ ) and **FcBF<sub>4</sub>** (10.9 mg, 40  $\mu\text{mol}$ ) were partially dissolved in  $\text{CH}_2\text{Cl}_2$  (2 mL) with rapid stirring. After 1 min, the solution was treated dropwise with **dpe** (8.0 mg, 20  $\mu\text{mol}$ ) in  $\text{CH}_2\text{Cl}_2$  (0.5 mL). The solution was stirred for another 0.5 min, pentane ( $-28 \text{ }^\circ\text{C}$ , 15 mL) was added, and the mixture was allowed to stand at  $-28 \text{ }^\circ\text{C}$  for 10 min. The solids were isolated by filtration, washed with pentane ( $-28 \text{ }^\circ\text{C}$ ,  $2 \times 2 \text{ mL}$ ), and dried briefly to afford the title compound (16.4 mg, 13.2  $\mu\text{mol}$ , 66%) as an orange powder.

FT-IR:  $\nu_{\text{CO}} = 1967 \text{ cm}^{-1}$ . <sup>31</sup>P{<sup>1</sup>H} NMR ( $\text{CD}_2\text{Cl}_2$ , 202 MHz) 59.5, 58.3 ppm. Anal. Calcd for  $\text{C}_{57}\text{H}_{54}\text{B}_2\text{F}_8\text{FeNiO}_2\text{P}_4\text{S}_2$ : C, 54.89; H, 4.36; N, 0.00. Found: C, 54.77; H, 4.41; N, 0.00.

Orange prismatic single crystals of **[5](BF<sub>4</sub>)<sub>2</sub>·4CH<sub>2</sub>Cl<sub>2</sub>** were grown by layering a concentrated  $\text{CH}_2\text{Cl}_2$  solution with pentane and allowing the mixture to stand at  $-28 \text{ }^\circ\text{C}$ . One crystal ( $0.261 \times 0.237 \times 0.108 \text{ mm}^3$ ) was subjected to X-ray diffraction at 193 K. Its space group was determined to be triclinic  $P\bar{1}$  with cell parameters:  $a = 16.680 \text{ \AA}$ ,  $b = 14.195 \text{ \AA}$ ,  $c = 21.288 \text{ \AA}$ ,  $\alpha = 78.98^\circ$ ,  $\beta = 75.07^\circ$ ,  $\gamma = 64.26^\circ$ . Integration of 9944 reflections and solution by direct methods using SHELXTL V6.12<sup>50,51</sup> afforded a model with  $R1 = 0.0465$  and  $wR2 = 0.1126$ .

## CALCULATIONS

Calculations of structural parameters and the electronic structure were performed using ORCA.<sup>52</sup> Geometry optimizations were performed using the BP86 exchange–correlation functional<sup>30,31</sup> and a triple- $\zeta$  basis set with polarization functions that were obtained from the TURBOMOLE<sup>53</sup> library. This combination of exchange–correlation functional and basis set was shown to give accurate structural parameters. In addition, single-point calculations using the hybrid B3LYP<sup>32</sup> and PBE0<sup>33,34</sup> functionals on the BP86/TZVP geometry optimized structures were carried out. This combination of exchange–correlation functional and basis set was shown to give accurate structural parameters. IR spectra were generated by numerically calculating second derivatives; calculations of *g*-tensors were performed using an effective mean-field spin–orbit coupling operator, with the center-of-mass as the origin



of the  $g$ -tensor.<sup>54</sup> Additional  $g$ - and  $A$ -tensor calculations were performed with ADF<sup>54,56</sup> using the zero-order regular approximation (ZORA)<sup>57</sup> for relativistic effects and a self-consistent inclusion of spin-orbit coupling. A Slater-orbital DZ basis set was used for spin-restricted  $g$ -tensor calculations,<sup>58</sup> and a TZP basis set was used for spin-unrestricted scalar relativistic hyperfine and quadrupole coupling tensor calculations.<sup>59,60</sup>

## ■ ASSOCIATED CONTENT

### ■ Supporting Information

Spectroscopy results and calculated  $g$ -tensor values for the studied compounds. This material is available free of charge via the Internet at <http://pubs.acs.org>.

## ■ ACKNOWLEDGMENTS

The authors wish to thank Bryan Barton for helpful discussions and Drs. Danielle L. Gray and Amy L. Fuller for X-ray crystallography. This work was supported by the National Institutes of Health (Grants GM061153 to T.R., GM46441 and GM084266 to P.L.).

## ■ REFERENCES

- (1) Liu, T.; Darensbourg, M. Y. *J. Am. Chem. Soc.* **2007**, *129*, 7008.
- (2) Justice, A. K.; De Gioia, L.; Nilges, M. J.; Rauchfuss, T. B.; Wilson, S. R.; Zampella, G. *Inorg. Chem.* **2008**, *47*, 7405.
- (3) Justice, A. K.; Nilges, M.; Rauchfuss, T. B.; Wilson, S. R.; De Gioia, L.; Zampella, G. *J. Am. Chem. Soc.* **2008**, *130*, 5293.
- (4) Lacey, A. L. D.; Fernández, V. M.; Rousset, M.; Cammack, R. *Chem. Rev.* **2007**, *107*, 4304.
- (5) Ogata, H.; Lubitz, W.; Higuchi, Y. *Dalton Trans.* **2009**, 7577.
- (6) Chapman, A.; Cammack, R.; Hatchikian, C. E.; McCracken, J.; Peisach, J. *FEBS Lett.* **1988**, *242*, 134.
- (7) Whitehead, J. P.; Gurbel, R. J.; Bagyinka, C.; Hoffman, B. M.; Maroney, M. J. *J. Am. Chem. Soc.* **1993**, *115*, 5629.
- (8) van der Zwaan, J. W.; Albracht, S. P. J.; Fontijn, R. D.; Slater, E. C. *FEBS Lett.* **1995**, *179*, 271.
- (9) Stein, M.; Lubitz, W. *Phys. Chem. Chem. Phys.* **2001**, *3*, 5115.
- (10) Volbeda, A.; Charon, M.-H.; Piras, C.; Hatchikian, E. C.; Frey, M.; Fontecilla-Camps, J. C. *Nature* **1995**, *373*, 580.
- (11) Volbeda, A.; Martin, L.; Cavazza, C.; Matho, M.; Faber, B. W.; Roseboom, W.; Albracht, S. P. J.; Garcin, E.; Rousset, M.; Fontecilla-Camps, J. C. *J. Biol. Inorg. Chem.* **2005**, *10*, 239.
- (12) Higuchi, Y.; Ogata, H.; Miki, K.; Yasuoka, N.; Yagi, T. *Structure* **1999**, *7*, 549.
- (13) Higuchi, Y.; Yagi, T.; Yasuoka, N. *Structure* **1997**, *5*, 1671.
- (14) Matias, P. M.; Soares, C. M.; Saraiva, L. M.; Coelho, R.; Morais, J.; Gall, J. L.; Carrondo, M. A. *J. Biol. Inorg. Chem.* **2001**, *6*, 63.
- (15) Happe, R. P.; Roseboom, W.; Pierik, A. J.; Albracht, S. P. J.; Bagley, K. A. *Nature* **1997**, *385*, 126.
- (16) Tanino, S.; Li, Z.; Ohki, Y.; Tatsumi, K. *Inorg. Chem.* **2009**, *48*, 2358.
- (17) Ogata, H.; Mizoguchi, Y.; Mizuno, N.; Miki, K.; Adachi, S.-i.; Yasuoka, N.; Yagi, T.; Yamauchi, O.; Hirota, S.; Higuchi, Y. *J. Am. Chem. Soc.* **2002**, *124*, 11628.
- (18) Jiang, J.; Maruani, M.; Solaimanzadeh, J.; Lo, W.; Koch, S. A.; Millar, M. *Inorg. Chem.* **2009**, *48*, 6359.
- (19) Zhu, W.; Marr, A. C.; Wang, Q.; Neese, F.; Spencer, D. J. E.; Blake, A. J.; Cooke, P. A.; Wilson, C.; Schröder, M. *Proc. Natl. Acad. Sci. U.S.A.* **2005**, *102*, 18280.
- (20) Barton, B. E.; Whaley, C. M.; Rauchfuss, T. B.; Gray, D. L. *J. Am. Chem. Soc.* **2009**, *131*, 6942.
- (21) Barton, B. E.; Rauchfuss, T. B. *J. Am. Chem. Soc.* **2010**, *132*, 14877.
- (22) Telsler, J.; Benecky, M. J.; Adams, M. W. W.; Mortenson, L. E.; Hoffman, B. M. *J. Biol. Chem.* **1986**, *261*, 13536.
- (23) Carroll, M. E.; Barton, B. E.; Gray, D. L.; Mack, A. E.; Rauchfuss, T. B. *Inorg. Chem.* **2011**, *50*, 9554.
- (24) MacNeil, J. H.; Chiverton, A. C.; Fortier, S.; Baird, M. C.; Hynes, R. C.; Williams, A. J.; Preston, K. F.; Ziegler, T. *J. Am. Chem. Soc.* **1991**, *113*, 9834.
- (25) Justice, A. K.; Gioia, L. D.; Nilges, M. J.; Rauchfuss, T. B.; Wilson, S. R.; Zampella, G. *Inorg. Chem.* **2008**, *47*, 7405.
- (26) Thomas, C. M.; Liu, T.; Hall, M. B.; Darensbourg, M. Y. *Inorg. Chem.* **2008**, *47*, 7009.
- (27) Tolman, C. A. *Chem. Rev.* **1977**, *77*, 313.
- (28) Bertini, L.; Greco, C.; Bruschi, M.; Fantucci, P.; de Gioia, L. *Organometallics* **2010**, *29*, 2013.
- (29) Liu, T.; Li, B.; Singleton, M. L.; Hall, M. B.; Darensbourg, M. Y. *J. Am. Chem. Soc.* **2009**, *131*, 8296.
- (30) Becke, A. D. *Phys. Rev. A* **1988**, *38*, 3098.
- (31) Perdew, J. P. *Phys. Rev. B* **1986**, *33*, 8822.
- (32) Stephens, P. J.; Devlin, F. J.; Chabalowski, C. F.; Frisch, M. J. *J. Phys. Chem.* **1994**, *98*, 11623.
- (33) Ernzerhof, M.; Scuseria, G. *J. Chem. Phys.* **1999**, *110*, 5029.
- (34) Adamo, C.; Barone, V. *J. Chem. Phys.* **1999**, *110*, 6158.
- (35) Song, L.-C.; Li, Q.-S.; Yang, Z.-Y.; Hua, Y.-J.; Bian, H.-Z.; Hu, Q.-M. *Eur. J. Inorg. Chem.* **2010**, 1119.
- (36) Apfel, U.-P.; Troegel, D.; Halpin, Y.; Tschierlei, S.; Uhlemann, U.; Görls, H.; Schmitt, M.; Popp, J.; Dunne, P.; Venkatesan, M.; Coey, M.; Rudolph, M.; Vos, J. G.; Tacke, R.; Weigand, W. *Inorg. Chem.* **2010**, *49*, 10117.
- (37) Redin, K.; Wilson, A. D.; Newell, R.; Rakowski DuBois, M.; DuBois, D. L. *Inorg. Chem.* **2007**, *46*, 1268.
- (38) Lubitz, W.; Reijerse, E.; van Gestel, M. *Chem. Rev.* **2007**, *107*, 4331.
- (39) Lacey, A. L. D.; Stadler, C.; Fernandez, V. M.; Hatchikian, E. C.; Fan, H. J.; Li, S. H.; Hall, M. B. *J. Biol. Inorg. Chem.* **2002**, *7*, 318.
- (40) van der Zwaan, J. W.; Albracht, S. P. J.; Fontijn, R. D.; Roelofs, Y. B. *Biochim. Biophys. Acta* **1986**, *872*, 208.
- (41) Pandelia, M.-E.; Ogata, H.; Currell, L. J.; Flores, M.; Lubitz, W. *Biochim. Biophys. Acta* **2010**, *1797*, 304.
- (42) Pandelia, M.-E.; Ogata, H.; Lubitz, W. *ChemPhysChem* **2010**, *11*, 1127.
- (43) Foerster, S.; Stein, M.; Brecht, M.; Ogata, H.; Higuchi, Y.; Lubitz, W. *J. Am. Chem. Soc.* **2003**, *125*, 83.
- (44) Bennett, B.; Lemon, B. J.; Peters, J. W. *Biochemistry* **2000**, *39*, 7455.
- (45) Popescu, C. V.; Münck, E. *J. Am. Chem. Soc.* **1999**, *121*, 7877.
- (46) Fiedler, A. T.; Brunold, T. C. *Inorg. Chem.* **2005**, *44*, 9322.
- (47) Razavet, M.; Davies, S. C.; Hughes, D. L.; Barclay, J. E.; Evans, D. J.; Fairhurst, S. A.; Liu, X. M.; Pickett, C. J. *J. Chem. Soc., Dalton Trans.* **2003**, 586.
- (48) Pereira, A. S.; Tavares, P.; Moura, I.; Moura, J. J. G.; Huynh, B. H. *J. Am. Chem. Soc.* **2001**, *123*, 2771.
- (49) Rauchfuss, T. B. *Inorg. Chem.* **1977**, *16*, 2966.
- (50) Sheldrick, G. M. *Acta Crystallogr.* **2008**, *A64*, 112.
- (51) SHELXTL, Bruker AXS, I., Madison, Wisconsin, USA.
- (52) Neese, F., ORCA - An ab initio, DFT and semiempirical SCF-MO package, version 2.8.0, University of Bonn, Bonn, Germany.
- (53) Schaefer, A.; Huber, C.; Ahlrichs, R. *J. Chem. Phys.* **1994**, *100*, 5829. And <ftp.chemie.uni-karlsruhe.de/pub/basen>.
- (54) Ruud, K.; Vaara, J.; Lounila, J.; Helgaker, T. *Chem. Phys. Lett.* **1998**, *297*, 467. Neese, F. *J. Chem. Phys.* **2001**, *115*, 11080. Neese, F. *J. Chem. Phys.* **2005**, *122*, 034107.
- (55) te Velde, G.; Bickelhaupt, F. M.; van Gisbergen, S. J. A.; Guerra, C. F.; Baerends, E. J.; Snijders, J. G.; Ziegler, T. *J. Comput. Chem.* **2001**, *22*, 931.
- (56) ADF2010, SCM, Theoretical Chemistry, Vrije Universiteit, Amsterdam, The Netherlands.
- (57) van Lenthe, E.; Baerends, E. J.; Snijders, J. G. *J. Chem. Phys.* **1993**, *99*, 4597.
- (58) van Lenthe, E.; van der Avoird, A.; Wormer, P. E. S. *J. Chem. Phys.* **1997**, *107*, 2488.
- (59) van Lenthe, E.; van der Avoird, A.; Wormer, P. E. S. *J. Chem. Phys.* **1998**, *108*, 4783.
- (60) van Lenthe, E.; Baerends, E. J. *J. Chem. Phys.* **2000**, *112*, 8279.